Stem Cell Reports
Article
ISSCR
OPEN ACCESS

# Modulation of the canonical Wnt activity by androgen signaling in prostate epithelial basal stem cells

Corrigan Horton,[1,3] Yueli Liu,[1,3] Jiawen Wang,[2] Jonathan Green,[1] Jeremiah Tsyporin,[1] Bin Chen,[1] and Zhu A. Wang[1,*]
[1]Department of Molecular, Cell, and Developmental Biology, University of California, Santa Cruz, Santa Cruz, CA 95064, USA
[2]Sequencing Center, National Institute of Biological Sciences, Beijing 102206, China
[3]These authors contributed equally
*Correspondence: zwang36@ucsc.edu
https://doi.org/10.1016/j.stemcr.2023.04.003

## SUMMARY

Both the canonical Wnt and androgen receptor (AR) signaling pathways are important for prostate organogenesis and homeostasis. How they crosstalk to regulate prostate stem cell behaviors remains unclear. Here, we show in lineage-tracing mouse models that although Wnt is essential for basal stem cell multipotency, ectopic Wnt activity promotes basal cell over-proliferation and squamous phenotypes, which are counteracted by elevated levels of androgen. In prostate basal cell organoids, dihydrotestosterone (DHT) antagonizes R-spondin-stimulated growth in a concentration-dependent manner. DHT down-regulates the expressions of a Wnt reporter and target genes, and RNA sequencing (RNA-seq) analyses identify Wnt signaling as a key altered pathway. Mechanistically, DHT enhances AR and β-catenin protein binding, and CUT&RUN analyses reveal that ectopic AR sequesters β-catenin away from its Wnt-related cistrome. Our results suggest that an intermediate level of Wnt activity in prostate basal stem cells, achieved via AR-β-catenin interaction, is essential for normal prostate homeostasis.

## INTRODUCTION

Signaling crosstalk is crucial for regulating adult stem cell in an organ. The canonical Wnt signaling pathway is a key player in stem cell self-renewal and differentiation in multiple tissues (Holland et al., 2013; Clevers et al., 2014). Its interaction with hormone signals may be important for orchestrating the behaviors of adult stem cells in tissues under hormonal regulation. In the prostate gland, both Wnt and androgen receptor (AR) signaling pathways are essential for driving organogenesis (Toivanen and Shen, 2017). Specifically, stromal Wnt secretion promotes prostate bud branching morphogenesis and expression of the prostate-specific transcription factor Nkx3.1 in the epithelium (Simons et al., 2012; Francis et al., 2013; Julio et al., 2013). Classical tissue recombination experiments and conditional knockout experiments have revealed the requirement of stromal AR in instructing the specification of prostate epithelium through paracrine signals (Cunha et al., 1992; Lai et al., 2012). However, how Wnt and androgen signals interact to regulate prostate development and whether the interaction affects prostate stem cells remain unclear.

Basal and luminal cells are the two major cell types lining the prostate epithelium. Lineage-tracing analysis showed that during prostate organogenesis, basal cells behave as stem cells to rapidly proliferate and generate luminal cells (Ousset et al., 2012). Using organoid culture, basal cells were found to be more efficient than luminal cells in generating prostate organoids (Karthaus et al., 2014). The standard organoid culture medium contains R-spondin, an agonist of the canonical Wnt pathway (Binnerts et al., 2007), indicating a role of Wnt signaling for enhancing prostate basal stem cell functions. In support of this, conditional knockout of β-catenin in basal cells during prostate postnatal development appeared to negatively affect their luminal differentiation (Lu and Chen, 2015). However, basal stem cells display high plasticity, as they become more restricted in the adult prostate, with basal-to-luminal differentiation occurring infrequently during homeostasis (Choi et al., 2012; Wang et al., 2013) and reactivated only in epithelium injury repair (Toivanen et al., 2016; Horton et al., 2019). It was reported that epithelial β-catenin was not required for maintaining the overall normal morphology of the adult prostate (Francis et al., 2013), but whether/how Wnt signaling regulates adult prostate basal stem cells has not been specifically examined.

Recently, our lab performed basal cell lineage tracing with AR conditional knockout in long-term prostate homeostasis, and demonstrated that AR within adult basal cells is dispensable for their maintenance, but required for basal-to-luminal cell differentiation *in vivo* (Xie et al., 2017). This led us to ask whether Wnt signaling in adult basal cells plays similar roles. In addition, it remains to be studied whether crosstalk between the Wnt and AR signaling pathways is involved in regulating the plasticity of basal stem cells. In this study, we show that Wnt activity levels in prostate basal cells need to be tightly controlled in prostate homeostasis, and that androgen signaling can down-regulate Wnt activity through AR sequestering β-catenin away from its Wnt target genes.

## RESULTS

### Canonical Wnt activity is essential for prostate basal-to-luminal cell differentiation in homeostasis but not in cancer initiation

Given that basal stem cells show plasticity as prostate matures, we examined Wnt signaling activities at developmental and adult stages using the *TCF/Lef-H2B.GFP* reporter mice (Ferrer-Vaquer et al., 2010). At postnatal day 20 (P20), we observed robust GFP expression in stromal cells as well as basal cells at the ductal tips (Figure S1A). In contrast, by P50, GFP was absent in basal cells and sporadic in stromal cells, but highly turned on in luminal cells (Figure S1B). Therefore, restriction of basal stem cells in the adult prostate coincides with their decreased Wnt activities. To functionally test the role of Wnt signaling in adult prostate basal cells, we performed β-catenin deletion in basal cells during long-term homeostasis. *CK5-CreER$^{T2}$* and *R26R-CAG-YFP/+* mouse lines were used to lineage-label all prostate basal cells, as shown previously (Xie et al., 2017). We tamoxifen-induced *CK5-CreER$^{T2}$; Ctnnb1$^{fl/fl}$; R26R-CAG-YFP/+* male mice (termed *Bas$^{bcat-/-}$*) and *CK5-CreER$^{T2}$; R26R-CAG-YFP/+* controls (termed *Bas$^{WT}$*) at 2 months of age and waited 6 months before analysis (Figure 1A). As β-catenin is expressed on the membrane of luminal cells, which contact the basal layer, its loss in individual basal cells could not be easily identified by immunofluorescence (IF) staining (Figure S2A). Nevertheless, efficient β-catenin deletion by *CK5-CreER$^{T2}$* was confirmed by flow sorting of YFP+ prostate basal cells from *Bas$^{bcat-/-}$* mice (Figure S2B) for qRT-PCR analysis (Figure S2C), inferred by observing hair loss through time (Figure S2D) (Kishimoto et al., 2000), and observed in basal-derived *bcat−/−Pten−/−* luminal cells described below (Figure 1H). Six months after induction, basal-to-luminal cell differentiation was significantly reduced in the *Bas$^{bcat-/-}$* group compared with *Bas$^{WT}$* (Figures 1B and 1C), while basal cell proliferation rates were unchanged as measured by Ki67 staining and BrdU incorporation assay (Figures 1D and 1E). These data suggest that the canonical Wnt signaling activities are dispensable for adult prostate basal cell maintenance but necessary for basal-to-luminal cell differentiation.

We next tested whether Wnt activities in basal cells are important for prostate cancer initiation by analyzing *CK5-CreER$^{T2}$; Pten$^{fl/fl}$; R26R-CAG-YFP/+* (*Bas$^{Pten-/-}$*) and *CK5-CreER$^{T2}$; ctnnb1$^{fl/fl}$; Pten$^{fl/fl}$; R26R-CAG-YFP/+* (*Bas$^{bcat-/-Pten-/-}$*) tumors at 3 and 6 months after tamoxifen induction (Figure 1A). We found that β-catenin deletion did not attenuate the progression of basal-derived *Pten*-null tumors, as *Bas$^{bcat-/-Pten-/-}$* were morphologically indistinguishable from the previously described *Bas$^{Pten-/-}$* tumors (Wang et al., 2013) (Figure 1F). The double knockout tumors clearly displayed cribriform pattern and abundant basal-to-luminal cell differentiation (Figure 1G), despite their lack of β-catenin expression (Figure 1H), suggesting that loss of Pten can override the requirement of β-catenin in promoting basal-to-luminal cell differentiation.

### Ectopic Wnt activity promotes prostate basal cell overproliferation

To assess whether gain of Wnt signaling activity could enhance basal stem cell functions, we tamoxifen-induced *CK5-CreER$^{T2}$; APC$^{fl/fl}$; R26R-CAG-YFP/+* mice (termed *Bas$^{APC-/-}$*) and analyzed the prostate morphology 2 weeks later (Figure 2A), at which time these mice usually succumbed to rapidly developing tumors growing elsewhere because of the widespread activity of the *CK5* promoter. At this early time point, the morphology of the prostate epithelium appeared largely normal. However, we observed clones of prostate basal cells forming continuous sheets or stacking with each other, resembling squamous tumor phenotypes (Figure 2B). This is consistent with previous studies that showed squamous metaplasia foci in mice with activated Wnt signaling throughout the prostate epithelium by *Pb-Cre4* (Bruxvoort et al., 2007; Yu et al., 2009). Notably, the YFP+ cells were strictly basal and did not express the luminal marker CK18 (Figure 2C), indicating no basal-to-luminal differentiation. IF staining with Ki67 antibody showed that basal cells of *Bas$^{APC-/-}$* mice were more proliferative than those of wild-type (Figures 2D and 2E). To assess the long-term effects of ectopic Wnt activity in basal cells, we isolated *Bas$^{APC-/-}$* basal cells by flow sorting of YFP+ cells and recombined them with rat urogenital mesenchyme cells before grafting the tissue recombinants under the kidney capsule of immunodeficient mice (Figure 2A). Three months after renal grafting, we observed large prostatic tissues grown on the kidney, which were YFP positive (Figure 2F), and IF staining again revealed squamous basal cell phenotypes (Figure 2G). Taken together, our results suggest that canonical Wnt signaling activities in prostate basal cells are tightly controlled in the normal prostate *in vivo* and that intermediate Wnt activity levels are favorable for basal-to-luminal cell differentiation.

### DHT antagonizes Wnt-stimulated basal stem cell activities in organoids and *in vivo*

Given the pivotal role of AR signaling in prostate functions, we next investigated how AR and Wnt signaling pathways crosstalk to regulate prostate basal stem cells using a defined organoid culture protocol (Drost et al., 2016). We flow-sorted prostate basal cells from *Bas$^{WT}$* mice and cultured them under 6 conditions: (1) "basement medium" (BM) containing all the factors as described in the protocol except for dihydrotestosterone (DHT) and the Wnt

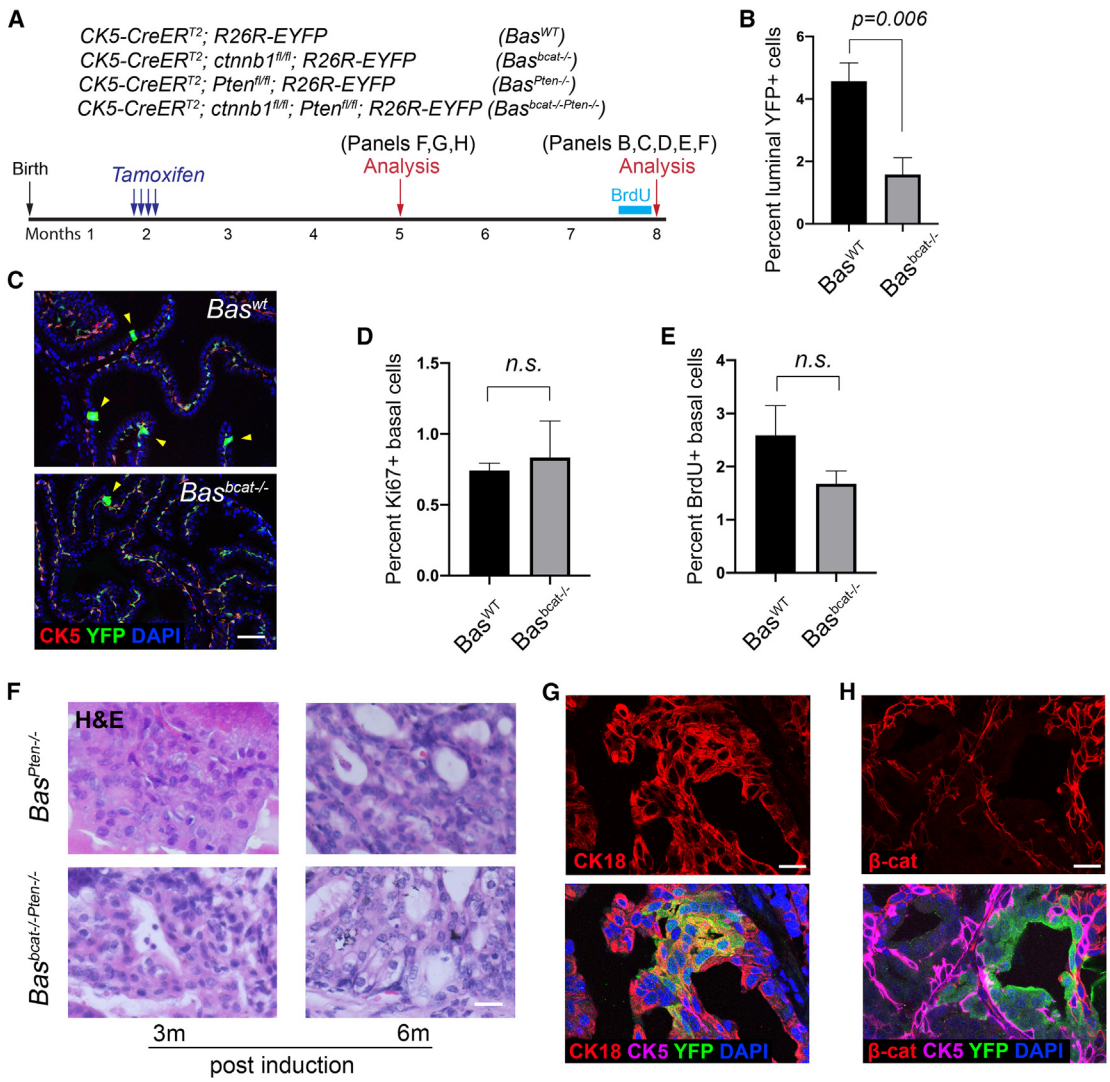


**Figure 1. Lineage-tracing analysis of *bcat−/−* basal cells during homeostasis and cancer initiation**

(A) Timeline for lineage tracing experiments.

(B) Comparing percentages of YFP$^+$ luminal cells from total YFP$^+$ cells in *Bas$^{WT}$* (N = 4 animals) and *Bas$^{bcat-/-}$* mice (N = 5 animals) at 6 months post-induction.

(C) Representative IF images of YFP$^+$ luminal cells (arrowheads) in the *Bas$^{WT}$* and *Bas$^{bcat-/-}$* prostate 6 months post-induction.

(D and E) Bar graphs showing no differences in proliferation rates between *Bas$^{WT}$* and *Bas$^{bcat-/-}$* basal cells by Ki67 (D) and BrdU (E) staining. N = 4 *Bas$^{WT}$* animals and 5 *Bas$^{bcat-/-}$* animals.

(F) Representative H&E images of *Bas$^{Pten-/-}$* and *Bas$^{Pten-/-;bcat-/-}$* prostate at 3 months and 6 months after tamoxifen induction.

(G and H) IF images showing increased basal-to-luminal differentiation (G) and loss of β-catenin (H) in *Bas$^{Pten-/-;bcat-/-}$* tumor regions at 3 months post-induction.

Scale bars, 50 μm (C) and 20 μm (F–H). Data were analyzed using Student's t test. Error bar denotes one SD.

potentiator R-spondin, (2) BM plus R-spondin (R), (3) BM plus $10^{-9}$ M DHT (DHT-9), (4) BM plus $10^{-7}$ M DHT (DHT-7), (5) BM plus R-spondin and $10^{-9}$ M DHT (RD-9), and (6) BM plus R-spondin and $10^{-7}$ M DHT (RD-7). Representative images of organoids growing for 7 days under different conditions are shown in Figure 3A. These organoids typically exhibit p63-expressing basal cells on the outskirt with intermediate and luminal cells in the center (Figure 3A). Organoids of R condition were more abundant than those of BM (Figure 3A), significantly larger (Figure 3B), and contained increased buds and surface complexity (Figure 3C), consistent with the notion that Wnt activity enhances basal stem cell activities and branching morphogenesis during organogenesis (Julio

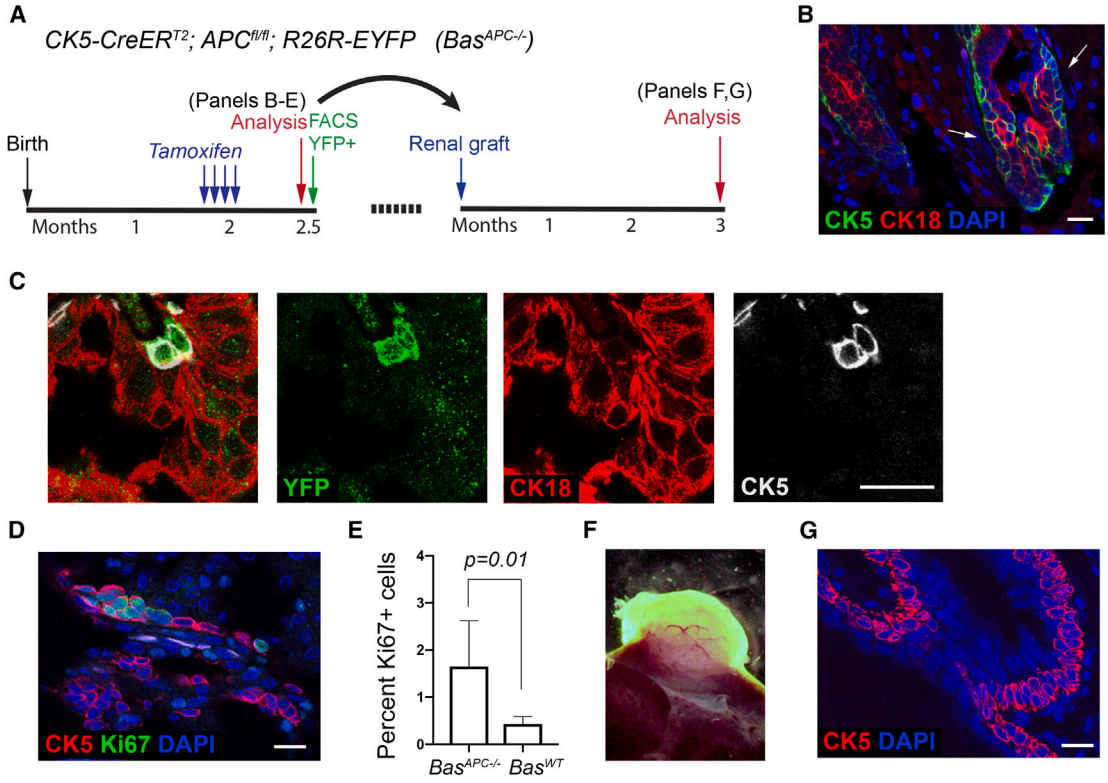


**Figure 2. *APC*$^{-/-}$ basal cells show over-proliferation and squamous phenotypes**

(A) Timeline of experiments for lineage tracing and renal grafting of *APC*$^{-/-}$ basal cells.

(B) Representative IF image showing squamous basal cell phenotype (arrows) in *Bas*$^{APC-/-}$ mice at 2 weeks post-induction.

(C) IF staining showing the strict basal cell identity of the YFP$^{+}$ cells in *Bas*$^{APC-/-}$ mice at 2 weeks post-induction.

(D) Over-proliferation of *APC*$^{-/-}$ basal cells shown by Ki67 staining.

(E) Bar graph comparing percentage of Ki67+ basal cells between *Bas*$^{APC-/-}$ mice and *Bas*$^{WT}$ mice. N = 3 animals for each. Data were analyzed using Student's t test. Error bar denotes one SD.

(F) Overlay image of white-field and YFP channels showing prostatic tissues attached to a piece of kidney.

(G) IF showing *Bas*$^{APC-/-}$ basal squamous phenotype in the renal graft tissues.

Scale bars, 20 μm (B–D and G).

et al., 2013). Interestingly, adding DHT suppressed basal stem cell activities in organoid culture in a concentration-dependent manner, as DHT-9 organoids showed significantly reduced number, sizes, and complexity compared with BM, while DHT-7 further exacerbated such phenotypes (Figures 3A–3C). DHT also antagonized the growth-promoting effects of R-spondin in a concentration-dependent manner, as the inhibitory effects were more prominent in RD-7 than RD-9 (Figures 3A–3C). These data imply that Wnt and androgen signaling pathways have opposite effects on prostate basal stem cell activities and that their combined effects may be subtractive.

To corroborate this finding *in vivo*, we implanted testosterone pumps onto tamoxifen-induced *Bas*$^{APC-/-}$ mice to assess the effects of ectopic androgen on Wnt-activated basal cells (Figure 3D). We analyzed the prostate tissues two weeks later and noticed a significant rescue of the squamous phenotype compared with control *Bas*$^{APC-/-}$ mice without pump implantation, as many basal cells were scattered and appeared normal in morphology (Figures 3E and 3F). Those basal cells also showed reduced proliferation (Figures 3E and 3G). Collectively, our data suggest that in both prostate organoids *in vitro* and homeostasis *in vivo*, androgen can antagonize Wnt-stimulated basal stem cell activities. Notably, despite this negative effect, androgen itself is required for basal-to-luminal cell differentiation (Xie et al., 2017). In both *Bas*$^{WT}$ and *Bas*$^{bcat-/-}$ mice that were castrated and lineage traced (Figure 3H), no YFP+ luminal cell was observed after prostate regression (Figure 3I), and basal cell proliferation rates were significantly reduced to almost zero compared with hormonal-intact state (Figures 3J and 3K), consistent with early reports (English et al., 1987; Evans and Chandler, 1987).

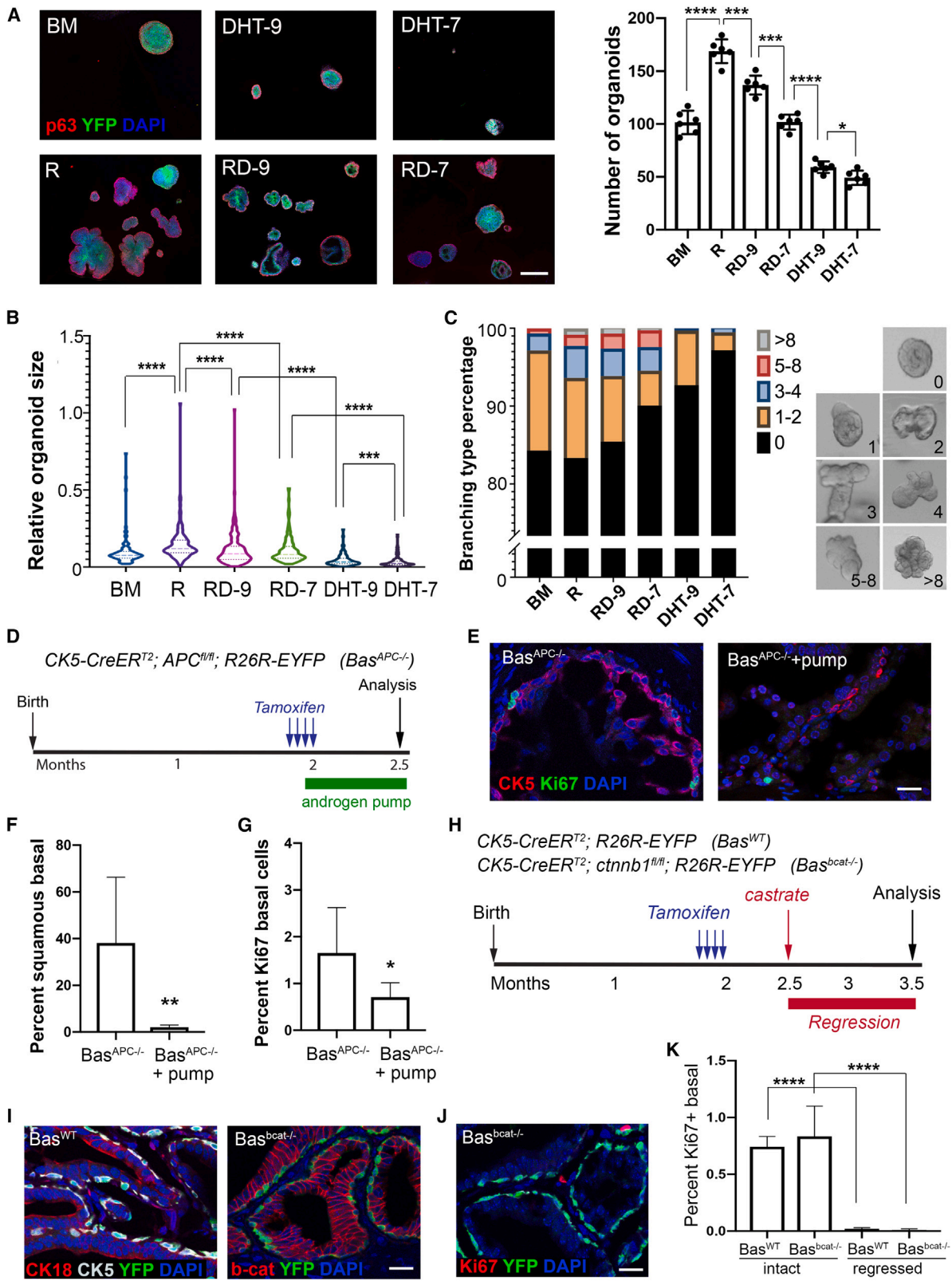


*(legend on next page)*

## DHT down-regulates Wnt signaling activities in prostate basal organoids

We hypothesized that DHT inhibits basal stem cell activities through inhibiting the canonical Wnt signaling pathway directly. To test it, we used cell surface markers $Lin^{-}CD49f^{hi}Sca\text{-}1^{+}$ to isolated basal cells (Xie et al., 2017) from the *TCF/Lef-H2B.GFP* reporter mice, and cultured them as organoids under BM, R, DHT-9, DHT-7, RD-9, and RD-7 conditions. Seven days later, we found that the GFP signals were most prominent in the R group, but almost absent in the DHT groups (Figure 4A). Quantitation of the percentage of GFP area of the organoids revealed the following trend: R > BM > RD-9 > RD-7 > DHT-9 > DHT-7 (Figure 4B), suggesting DHT down-regulates Wnt activities in a concentration-dependent manner. In further support, qRT-PCR analyses of several Wnt target genes *Axin2*, *Lef1*, *Ccnd2*, *Cd44*, and *Myc* showed lower expressions in RD-7 organoids compared with R (Figure S3A). These findings corroborate a previous study showing that androgen deprivation enhanced the Wnt reporter in LNCaP cells (Lee et al., 2015).

Next, we performed RNA sequencing (RNA-seq) for BM, R, and RD-7 organoids that had grown for 5 days. Principal-component analysis (PCA) and unsupervised hierarchical clustering analysis demonstrated the consistency of the samples within each group and the distinct transcriptomes of the RD-7 group from the BM and R groups (Figures 4C and 4D). Gene expression differential analysis revealed the numbers of up-regulated and down-regulated genes between each group (Figure S3B, Table S1). Many genes, including Wnt targets *Lgr5*, *Tcf7*, and *Wif1*, were up-regulated in R compared with BM but down-regulated in RD-7 compared with R (Figure S3C). Notably, the luminal marker gene *Nkx3.1* was highly up-regulated in RD-7, while the basal marker gene *Krt5* was down-regulated (Figure S3C), consistent with DHT's role in promoting basal-to-luminal differentiation. Gene Ontology (GO) analysis (Huang da et al., 2009) of differentially expressed genes between R and RD-7 identified key pathways involved, among which were cell cycle regulation and Wnt signaling pathway (Figure 4E), supporting our hypothesis that the inhibitory effects of androgen on basal organoids were mediated through modulation of the canonical Wnt activity, and corroborate a previous study comparing gene profiles of enzalutamide versus DHT-treated LNCaP cells (Guerrero et al., 2013). Moreover, gene set enrichment analysis (GSEA) (Subramanian et al., 2005) showed that genes that were up-regulated in RD-7 vs. R were highly enriched in two androgen-induced gene signatures published previously (Schaeffer et al., 2008; Mulholland et al., 2011) (Figure 4F). In contrast, genes that were down-regulated in RD-7 vs. R were highly enriched in the GO terms "Wnt receptor signaling pathway" and "organ morphogenesis" (Figure 4G). These findings support that androgen inhibits the canonical Wnt signaling activities in prostate basal stem cells.

## DHT increased AR and β-catenin protein binding in prostate organoid cells

Previous studies using prostate cancer cell lines have shown that AR can compete with TCF for β-catenin binding in the presence of androgen, and that the binding of β-catenin to AR can enhance AR signaling output (Terry et al., 2006). How AR and β-catenin binding affects Wnt signaling activity is unclear. We hypothesize that DHT inhibition of Wnt signaling activity in prostate basal cell organoids may be mediated through increased AR binding to β-catenin in the nucleus to sequester β-catenin away from carrying out its function as a Wnt pathway transcription factor (Figure 5A). To test this hypothesis, we first analyzed endogenous AR and β-catenin interactions by performing the Duolink Proximity Ligation Assay (PLA) (Fredriksson et al., 2002; Soderberg et al., 2008) in prostate basal organoids under different conditions. In PLA, antibodies recognizing two proteins that are in close proximity are

**Figure 3. DHT suppresses Wnt-induced basal stem cell activities *in vitro* and *in vivo***

(A) Representative IF images showing organoid morphology and bar graph showing organoid number per well under different culturing conditions (n = 6 wells from 3 batches cultured at different times for each condition). Scale bar, 200 μm. *p < 0.05, ***p < 0.001, and ****p < 0.0001, Student's t test. Error bar denotes one SD.

(B) Violin plot comparing relative organoid sizes under various conditions. ***p < 0.001 and ****p < 0.0001, Mann-Whitney U test.

(C) Quantification of organoid budding under various conditions. Examples of different numbers of buds shown on the right.

(D) Timeline of experiment for lineage tracing of $APC^{-/-}$ basal cells under androgen pump.

(E) Representative IF images comparing morphology and Ki67 positivity of $APC^{-/-}$ basal cells with or without androgen pump. Scale bar, 20 μm.

(F and G) Bar graphs comparing the percentages of basal cells with squamous phenotype (F) and Ki67 signal (G) between $Bas^{APC-/-}$ mice with or without pump. N = 3 animals for each group. *p < 0.05 and **p < 0.01, Student's t test. Error bar denotes one SD.

(H) Timeline of experiment for lineage tracing of castrated basal cells.

(I and J) Representative IF images showing no luminal YFP+ cells in regressed $Bas^{WT}$ and $Bas^{bcat-/-}$ mice (I) and no Ki67+ basal cells (J). Scale bars, 20 μm.

(K) Bar graph comparing basal cell proliferation before and after castration. N = 4, 5, 3, and 3 animals for each group, respectively. ****p < 0.0001, Student's t test. Error bar denotes one SD.

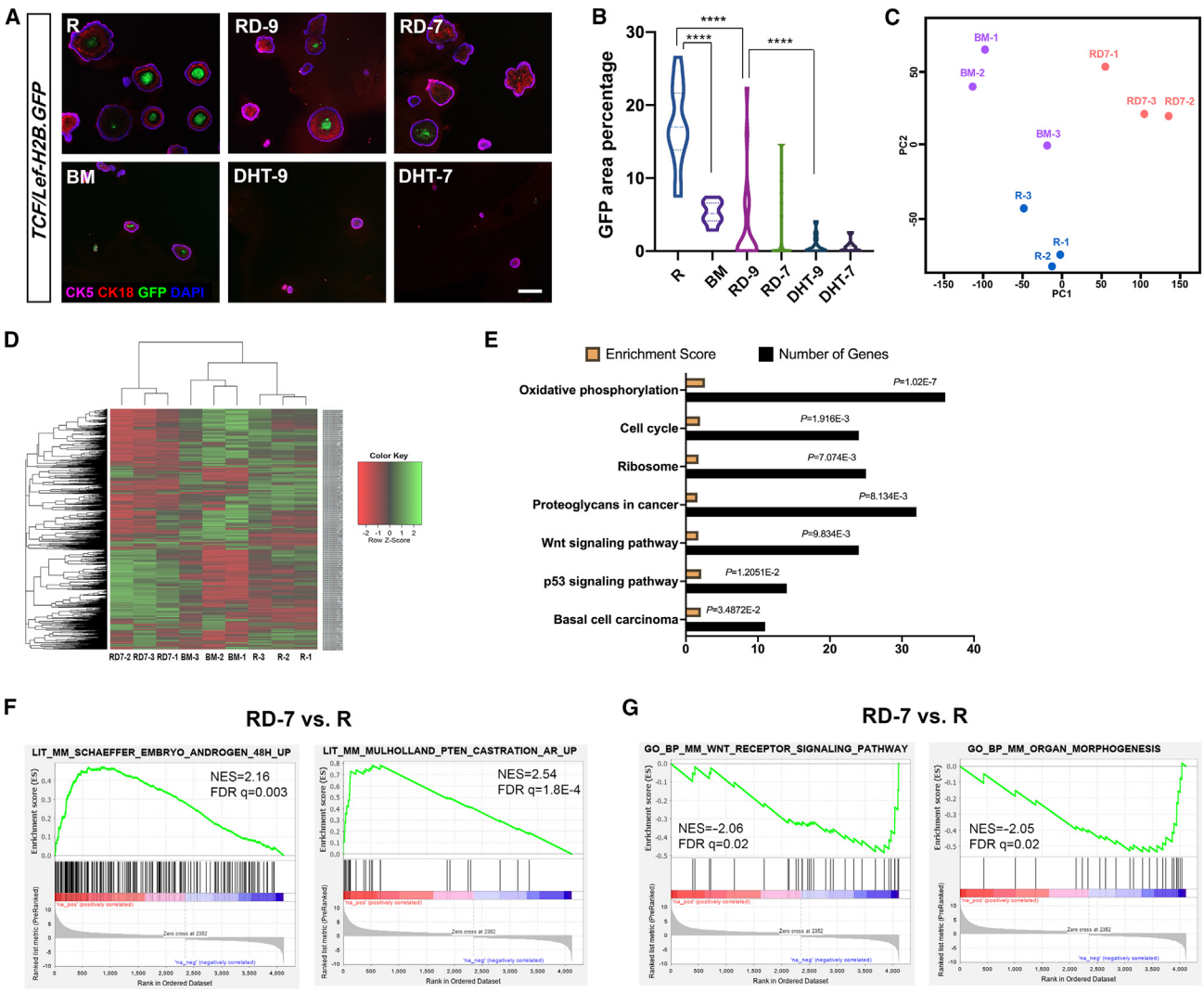


**Figure 4. DHT decreases Wnt signaling activities in prostate basal cell organoids**

(A) Representative IF images showing *TCF/Lef-H2B.GFP* reporter signals in basal-derived organoids cultured under different conditions. Scale bar, 200 μm.

(B) Violin plot showing GFP area percentages for different treatment conditions. Over 300 organoids cultured at 3 distinct batches were quantified for each condition. ****p < 0.0001, Mann-Whitney U test.

(C) Scatterplot of the two main components from a principal-component analysis of the BM (purple), R (blue), and RD-7 (orange) samples. n = 3 organoid samples in each group.

(D) Unsupervised hierarchical clustering analysis showing distinct transcriptomes of RD-7 from BM and R.

(E) GO analysis showing the enriched pathways in the comparison of R vs. RD-7, with the number of genes in each pathway.

(F and G) GSEA comparison of RD-7 vs. R showing androgen-responsive genes enriched in the up-regulated genes in the RD-7 group (F), and Wnt pathway genes and organ morphogenesis genes enriched in the down-regulated genes of the RD-7 group (G).

labeled with oligonucleotides and undertake rolling circle amplification to yield a specific fluorescent signal *in situ* (Figure 5B). In quality check experiments, we confirmed that PLA signals could only be detected when both AR and β-catenin antibodies were applied to the prostate organoids (Figure 5C). We then cultured the basal organoids for 7 days under BM, R, RD-9, and RD-7 conditions before performing Duolink PLA. The RD organoids clearly contained more signal dots than BM or R organoids (Figure 5D), and a positive correlation of the average number of signal dots per nucleus or per cell with the concentration of DHT was noted (Figure 5E). These data suggest that DHT promotes AR translocation into the nucleus and increases direct AR and β-catenin protein-protein interaction.

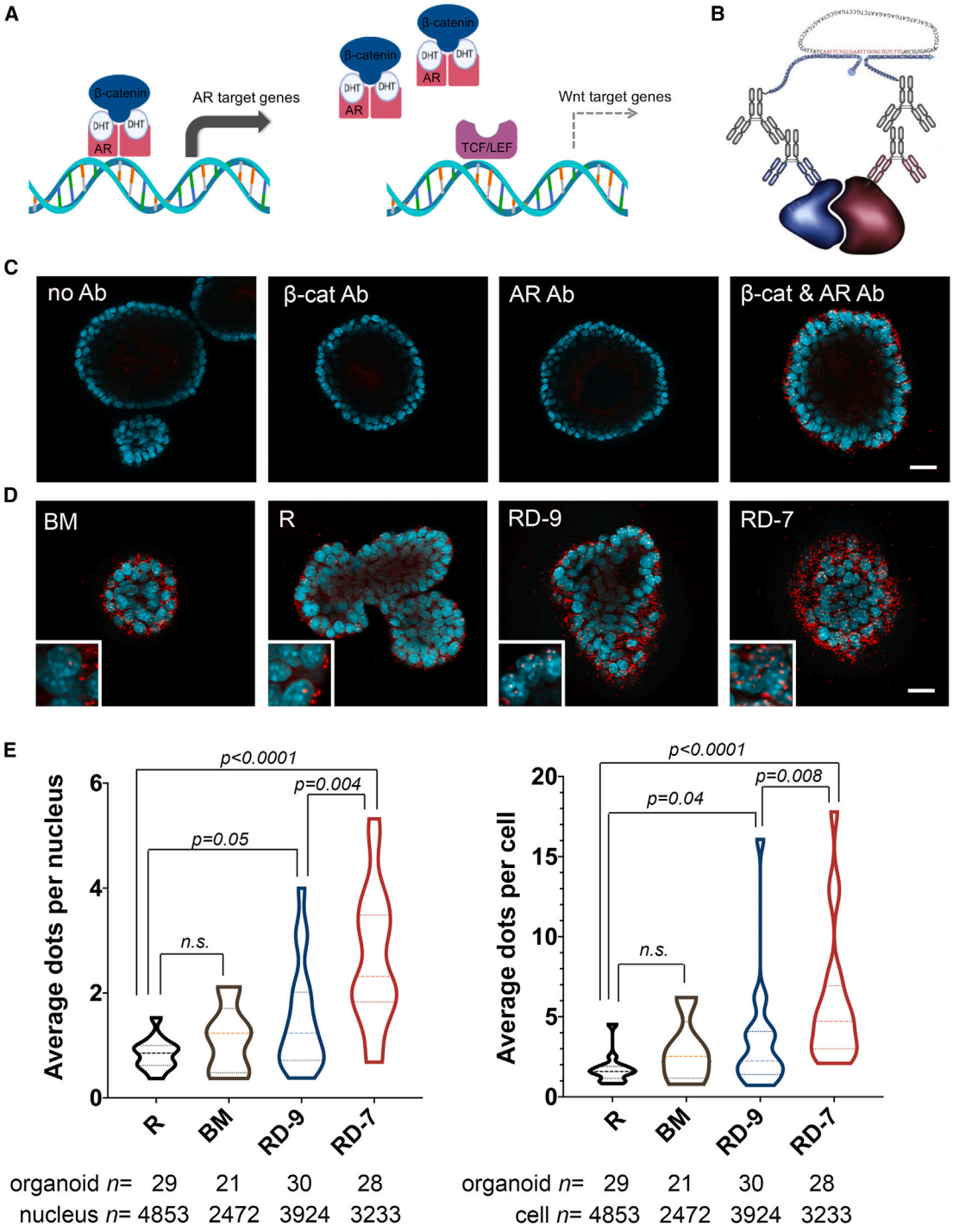


**Figure 5. Increased AR and β-catenin protein binding upon DHT treatment**

(A) Model of how AR and β-catenin interaction affects AR and Wnt signaling transcriptional output, respectively.

(B) Schematic diagram of the Duolink PLA for detecting protein interactions *in situ*.

(C and D) Representative IF images of prostate basal cell organoids showing positive Duolink PLA signals (red dots) only in the presence of both β-catenin and AR antibodies (C), and different signal densities under R, BM, RD-9, and RD-7 conditions (D). Insets show zoom-in views. Cyan represents nuclear DAPI staining. Scale bars, 50 μm.

*(legend continued on next page)*

### Analyses of AR and β-catenin cistromes under R and RD conditions

In order to test the model in Figure 5A and determine how Wnt signaling output was modified by increased AR-β-catenin binding, we next performed CUT&RUN (Skene and Henikoff, 2017) to characterize the AR and β-catenin cistromes in basal organoids cultured under the R and RD-7 conditions, resulting in 4 samples: R_AR, R_Bcat, RD_AR, and RD_Bcat. We called the peaks for each sample (Figure S4) and summarized the number of different and overlapping peaks among these samples in a Venn diagram (Figure 6A). These data showed that DHT shifted the binding patterns for both AR and β-catenin. Notably, when we ran the MEME motif analysis (Bailey et al., 2009; Machanick and Bailey, 2011) for the new AR binding peaks that were present in RD_AR but not R_AR (named Peak Set NewAR), the consensus AR binding motif was significantly enriched (Figure 6B), suggesting DHT promoted AR binding to androgen-responsive genes. We then performed GO pathway analysis for various β-catenin peak sets. Consistent with the role of R-spondin in promoting Wnt-induced basal stem cell activities, we found Kyoto Encyclopedia of Genes and Genomes (KEGG) pathway "Wnt signaling pathway" and GO term "multicellular organism development" to be among the top enriched pathways in R_Bcat peaks (Figure 6C). In contrast, for new β-catenin peaks that were present in RD_Bcat but not R_Bcat (named Peak Set NewBcat), GO terms "cell-cell adhesion" and "negative regulation of canonical Wnt signaling pathway," as well as KEGG pathway "cellular senescence" were significantly enriched (Figure 6C). Importantly, when we examined a subset of NewBcat that also contained AR co-localizing peaks in RD (named Peak Set NewCobind), the GO term "cell differentiation" was enriched, and "negative regulation of canonical Wnt signaling pathway" was enriched with an even greater enrichment score and a lower p value than in NewBcat (Figure 6C). These data support that DHT induced AR and β-catenin co-localization to regulatory genomic regions that negatively affected the canonical Wnt signaling activity.

To further test our model that AR sequesters β-catenin upon DHT treatment, we next compared β-catenin binding signals under R and RD conditions at defined AR peak sets. At those AR peaks that were present in R_AR but not RD_AR (named Peak Set OldAR, Figure 6B), there was no difference in β-catenin binding intensities between RD and R conditions (Figure 6D). This is consistent with our model, given that OldAR consists of AR binding sites that are not regulated by DHT but likely promoted by R-spondin. In contrast, across peaks in the NewAR set, we observed stronger β-catenin binding signals under RD condition compared with R (Figure 6E), suggesting that DHT-bound AR recruited β-catenin to the regulatory regions of those androgen-responsive genes. For example, RD_Bcat peaks co-localized with RD_AR peaks for AR target genes *Mme* and *Fkbp5*, while no R_Bcat peaks were present at those loci (Figure 6F). Furthermore, sequestration of β-catenin led to lower expressions of Wnt target genes such as stem cell markers *Cd44* and *Lgr5*, as the β-catenin peaks in R were lost in RD at those loci (Figure 6G). Taken altogether, our CUT&RUN data strongly support the model that androgen down-regulates Wnt signaling activity via AR sequestering β-catenin.

## DISCUSSION

Wnt signals have been shown to regulate epithelial stem cells in diverse tissues such as the intestine, mammary gland, and hair follicle (van Amerongen et al., 2012; Choi et al., 2013; Farin et al., 2016). The canonical Wnt signaling pathway is also essential for driving prostate branching morphogenesis (Francis et al., 2013; Julio et al., 2013), possibly through increasing basal stem cells. Indeed, prostate organoid growth from basal cells, a process that mimics early development, often entails adding the Wnt potentiator R-spondin in the culture medium (Drost et al., 2016). However, the adult prostate is a quiescent organ. During normal homeostasis, basal stem cells as illustrated by luminal differentiation capability only represent ~0.05% of the basal cells (Wang et al., 2013), and the basal stem cell program is reactivated in tumor initiation or in response to epithelium injury (Choi et al., 2012; Wang et al., 2013; Toivanen et al., 2016; Horton et al., 2019). This raises the question as to whether altered Wnt activities may underlie the plasticity of prostate basal stem cells. One piece of evidence comes from our observation comparing early and adult prostate using a Wnt reporter mouse line. Lineage-tracing analysis of β-catenin-null basal cells further supports this notion. Notably, our conclusion that Wnt is necessary for basal-to-luminal cell differentiation but not basal cell maintenance agrees with a previous linage-tracing study performed at postnatal stage (Lu and Chen, 2015). This suggests that Wnt activities are required for basal stem cell multipotency regardless of developmental stages, and that higher activities in early development are associated with more robust luminal cell

(E) Violin plots showing quantitation of average dots per nucleus (left) and dots per cell (right) in each organoid under different treatment conditions. Experiments were run in 3 independent batches, and the total numbers of organoids and cells analyzed for each condition are shown. p values were determined using the Mann-Whitney U test.

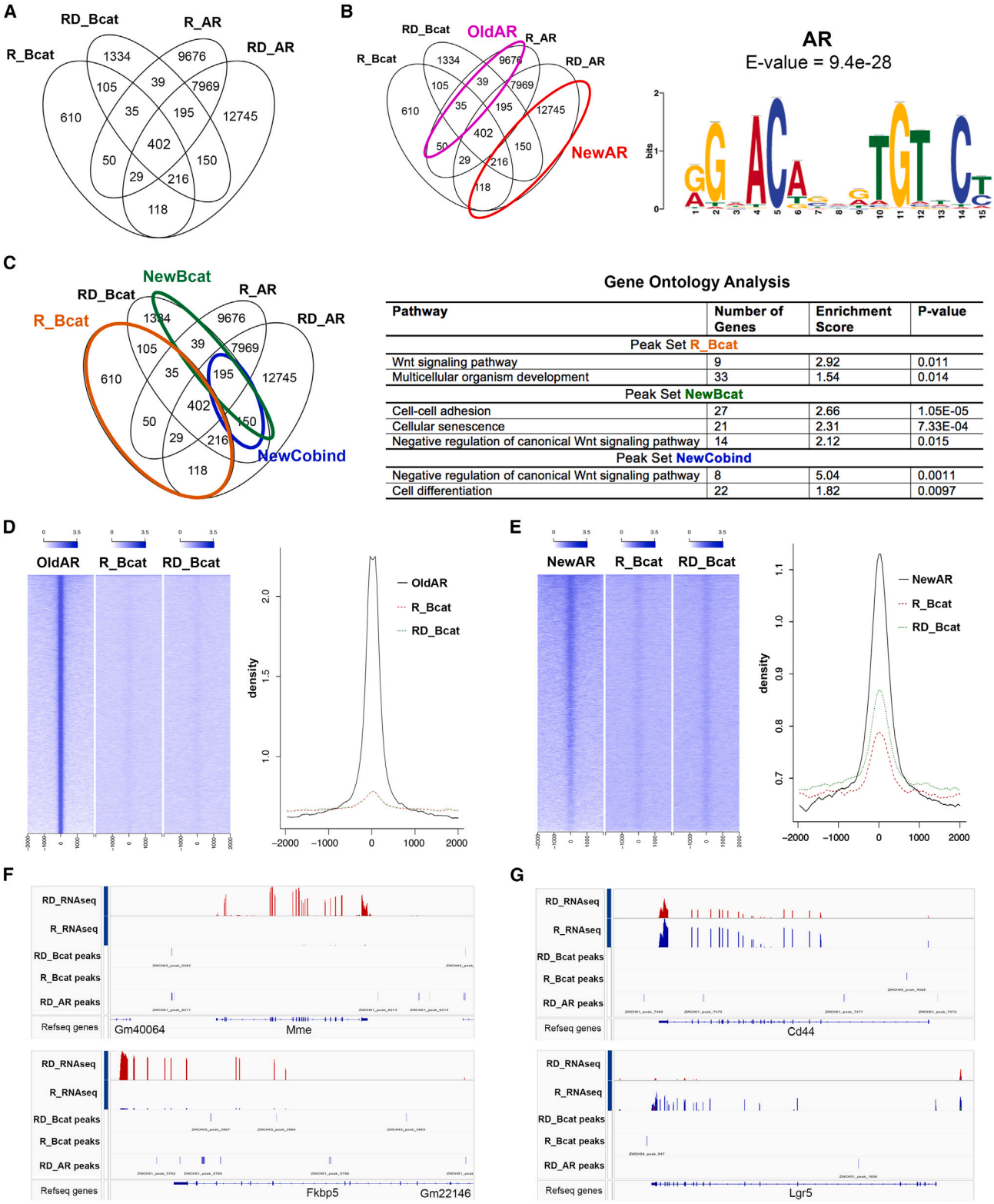


**Figure 6. CUT&RUN analyses of AR and β-catenin cistromes under R and RD conditions**

(A) Venn diagram showing the numbers of called peaks for each sample and peak overlaps among samples.

(B) Enrichment of the AR consensus motif in the NewAR peak set.

*(legend continued on next page)*

production. Such requirement can be overridden by activation of the PI3K pathway though, as our data showed no difference in luminal differentiation and tumor grades between $Bas^{Pten-/-}$ and $Bas^{bcat-/-Pten-/-}$ mice, contradicting the Lu study but consistent with another study knocking-out β-catenin and Pten using the *Pb-Cre* (Francis et al., 2013).

Although loss of Wnt activities hampers basal stem cell multipotency, ectopic Wnt through loss of APC induced basal cell over-proliferation and squamous phenotypes. This contrasts with the *Pten*-loss induced basal stem cell reactivation, where basal cell proliferation and basal-to-luminal differentiation dominate. We therefore propose that the behaviors of prostate basal stem cells can be regulated by Wnt signaling activities at three levels. Low levels of Wnt activities restrict basal stem cell proliferation and luminal differentiation in the adult prostate, while intermediate levels promote their stemness during prostate organogenesis and perhaps epithelium injury repair as well. Extreme high levels of Wnt activities, on the other hand, reprogram the normal basal cell identity to the one resembling squamous carcinoma. A recent study examining Wnt ligands expression *in situ* showed that stromal cells are a major source of various Wnts in both the early and adult prostate (Wei et al., 2022). Although the relative expression levels of Wnts could be a factor contributing to the distinct basal cell behaviors between developmental and adult stages, we provide evidence that AR signaling activities play an important role in modulating Wnt activities within basal cells. We show that DHT not only inhibited Wnt transcriptional output in basal cell organoids, but implanting testosterone pumps was able to reduce the squamous phenotypes induced by APC loss *in vivo*. In further support of our model, it has been reported that serum testosterone levels in mice greatly increase from birth onward and peak at P40 (Jean-Faucher et al., 1978; Poling and Kauffman, 2012). Such curvature overlaps with the decreasing stemness and Wnt activities of basal stem cells during prostate postnatal development. We also note that the apparent negative role of DHT on prostate organoid budding is not contradictory to the well-established notion that androgen signaling promotes prostate branching morphogenesis, because DHT directly works on basal cells in our organoid culture, while normal prostate epithelium development is promoted by stromal AR (Toivanen and Shen, 2017).

Mechanistically, we propose a model in which DHT-bound AR sequesters β-catenin away from activating Wnt target genes. Early studies in prostate cancer cell lines showed that β-catenin can bind to ligand-engaged AR protein and enhance the transcription of androgen-sensitive genes (Truica et al., 2000; Chesire et al., 2002; Mulholland et al., 2002; Pawlowski et al., 2002; Yang et al., 2002; Masiello et al., 2004). How this interaction affects the canonical Wnt signaling output has been less studied, but AR can compete with TCF for β-catenin binding, raising the possibility of suppressing Wnt target gene transcription (Amir et al., 2003; Mulholland et al., 2003; Song et al., 2003). For example, AR and LEF1 expressions were found to be mutually exclusive during branching morphogenesis and treatment with an AR antagonist resulted in Wnt/LEF1-positive basal progenitor repopulation of the luminal compartment (Wu et al., 2011). Recently, it was shown that androgen deprivation enhanced a Wnt reporter by increasing binding of β-catenin with TCF4 in LNCaP cells (Lee et al., 2015). Our findings extend on these prior studies, and provide new evidence in the prostate basal stem cell context. In particular, our CUT&RUN data indicated stronger β-catenin binding across the AR binding peaks of androgen-responsive genes in the presence of DHT, and weaker β-catenin binding at Wnt target genes including those involved in stem cell functions. Combined with our *in vivo* data, we propose that a relatively high Wnt/moderate androgen environment is permissible for prostate basal cells to function as active stem cells, low Wnt/high androgen for maintaining the quiescent basal cell state, and extreme high Wnt for altering the basal cell identity to a squamous cell type (Figure 7). In this model, the abundance of β-catenin and AR proteins in the basal cell nuclei regulates basal cell behaviors. More β-catenin will elevate the transcription of both AR and β-catenin target genes important for basal cell proliferation and luminal differentiation, until it reaches extreme where ectopic β-catenin target genes may be activated. On the other hand, more AR protein keeps basal cells in a quiescent state by activating genes for basal cell identity and sequestering β-catenin from turning on its normal targets. This model also explains the requirement of both AR (Xie et al., 2017) and β-catenin (this study) for basal-to-luminal differentiation, because complete loss of either one will lead to a subset of genes important for basal cell stemness being turned off.

(C) GO analysis showing selected enriched pathways for genes located in the peak sets R_Bcat, NewBcat, and NewCobind, respectively.
(D and E) Heatmaps and density plots comparing β-catenin binding intensities between R and RD conditions across the OldAR (D) and NewAR (E) binding peaks.
(F) Co-localization of AR and β-catenin binding peaks under RD condition at the *Mme* and *Fkbp5* gene loci (lower three rows by CUT&RUN). The upper two rows showing higher gene expression in RD vs. R by RNA-seq.
(G) Presence of β-catenin binding peaks in R but absence in RD at the *Cd44* and *Lgr5* gene loci. The upper two rows showing lower gene expression in RD vs. R by RNA-seq.

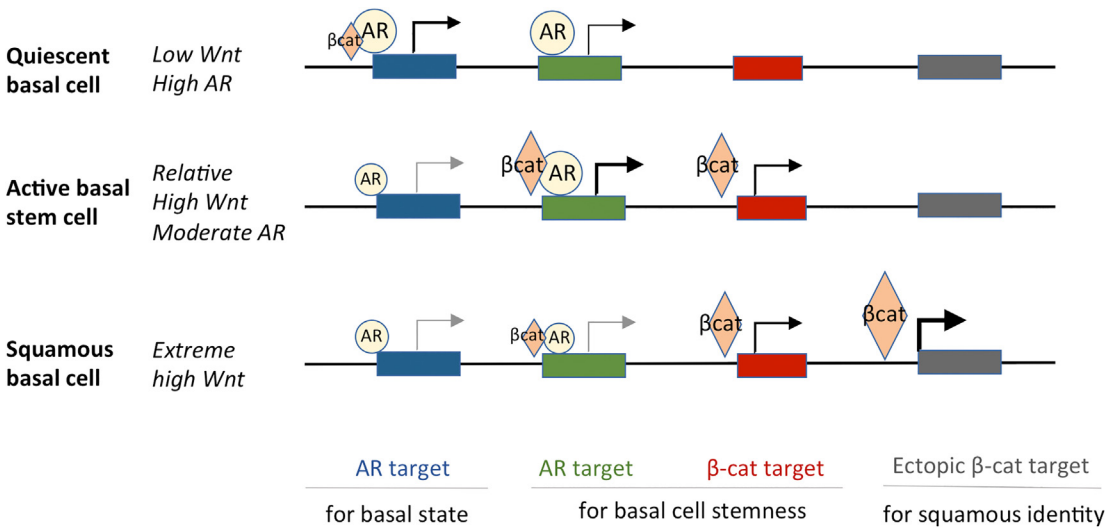


**Figure 7. Model of AR and β-catenin interaction in regulating prostate basal cell behaviors**

See text for details of the model. Different categories of transcriptional target genes are color-coded. For clarity, other transcription co-factors such as TCF/Lef are not shown. Size of the protein indicates its amount at the gene locus. Thickness of the arrow indicates target gene expression level.

Our findings were obtained from studying basal stem cells of the normal prostate, but may nevertheless have implications for prostatic diseases. It has been postulated that androgen signaling inhibits the transcription of Wnt target genes in hormone treatment naive prostate cancer (Yokoyama et al., 2014), while Wnt pathway activating mutations were found in 18% of the metastatic castration-resistant prostate cancer cases (Robinson et al., 2015). In an earlier disease context, reactivation of basal stem cells was found under the inflammatory condition (Kwon et al., 2013, 2016), and prostatitis is a significant etiologic factor in prostate cancer (De Marzo et al., 2007; Sfanos et al., 2018). We noticed that AR expression is often down-regulated in the inflammatory prostate epithelium (unpublished observation). It will be interesting to investigate whether the Wnt-AR cross-talk mechanism also applies under this scenario, as elevated Wnt activities could underlie the plasticity of basal stem cells in prostatitis. If so, it may provide new mechanistic insights into the link between prostatitis and prostate cancer.

## EXPERIMENTAL PROCEDURES

### Resource availability

#### *Corresponding author*

Further information and requests for resources and reagents should be directed to and will be fulfilled by the corresponding author, Zhu A. Wang (zwang36@ucsc.edu).

#### *Materials availability*

This study did not generate new unique reagents.

#### *Data and code availability*

All data reported in this paper will be shared by the corresponding author upon request. The prostate organoid RNA-seq data and CUT&RUN data are deposited in the Gene Expression Omnibus database with accession numbers GEO: GSE220499 and GEO: GSE220500, respectively.

This paper does not report original code.

Any additional information required to reanalyze the data reported in this paper is available from the corresponding author upon request.

### Mouse strains and genotyping

The *CK5-CreER$^{T2}$*, *Pten$^{flox}$*, and *R26R-CAG-YFP* lines were used previously (Xie et al., 2017). The *Ctnnb1$^{flox}$* (Brault et al., 2001) and *APC$^{flox}$* (Cheung et al., 2010) lines were obtained from JAX. The *TCF/Lef-H2B.GFP* line (Ferrer-Vaquer et al., 2010) was obtained from Dr. Hadjantonakis. Animals were maintained in C57BL/6N background. Genotyping was performed by PCR using tail genomic DNA, with the primer sequences listed in Table S2.

### Mouse procedures

Tamoxifen induction, BrdU labeling, and androgen pump implantation procedures were performed as described previously (Wang et al., 2013), and detailed in supplemental information. All animal experiments received approval from the Institutional Animal Care and Use Committee at the University of California, Santa Cruz (UCSC).

### Tissue collection and flow cytometry

Mouse prostate tissue dissection and flow cytometry were performed as previously described (Xie et al., 2017), and detailed in supplemental information. Lineage-marked basal cells were sorted on the basis of YFP positivity. Antibodies (Table S3) were used for

sorting Lin$^-$Sca-1$^+$ CD49f$^{hi}$ basal cells from *TCF/Lef-H2B.GFP* mice. Cell sorting was performed on a BD FACS Aria II instrument in the Flow Cytometry Facility of UCSC.

### Renal grafting assay

Renal grafting was performed as previously described (Horton et al., 2019), and detailed in supplemental information. Grafts were collected after 3 months of growth and embedded in OCT.

### Prostate organoids culture

Mouse prostate organoid culture medium was prepared according to a previous protocol (Drost et al., 2016), and detailed in supplemental information. Organoids were grown for 5–7 days before analyses to minimize the effects contributed by differentiated luminal cells. *In situ* organoid images and IF images were taken using a Keyence microscope and Zeiss AxioImager in the UCSC Microscopy Facility. For counting of organoid number, a minimum organoid diameter of 40 μm was considered. Organoid sizes and GFP area percentage were quantified using ImageJ.

### Histology and immunofluorescence staining

H&E and IF staining was performed using standard protocols as previously described (Xie et al., 2017) and detailed in supplemental information. Images were taken using a Zeiss AxioImager and a Leica TCS SP5 confocal microscope in the UCSC Microscopy Facility. All primary antibodies and dilutions used are listed in Table S3.

### qRT-PCR

Quantitative real-time PCR was carried out using Power SYBR Green PCR Master Mix (Life Technology) in the ViiA 7 Real-Time PCR instrument. Expression values were obtained using the ΔΔCT method and normalized to β-actin (*Actb*) expression; average values are shown as mean ± SD. Primer sequences are provided in Table S2.

### Duolink Proximity Ligation Assay

Duolink PLA was performed as per the kit instruction (DUO92101; Sigma-Aldrich), and repeated twice with consistent results. The antibodies used were AR (A9853; Sigma-Aldrich; rabbit, 1:500 dilution) and β-catenin (610153; BD Bioscience; mouse, 1:500 dilution). Images were taken using the Zeiss AxioImager. Quantitation of PLA signals was performed by manual counting the total number of dots in an organoid, the total number of dots within the nucleus (overlapping with DAPI), and the number of cells in an organoid. Average dots per cell/nucleus in an organoid were calculated and dozens of randomly selected organoids from each condition were imaged and counted.

### Lineage analysis and statistics

Identification of basal and luminal cells in lineage analysis was described previously (Xie et al., 2017) and detailed in supplemental information. Statistical analyses for lineage tracing and organoids experiments were performed using the two-sided Student's t test or the Mann-Whitney U test as appropriate. At least three biological replicates for each experiment or genotype were analyzed.

### Organoid bulk RNA-seq and analysis

Organoid mRNA was isolated using the RNeasy Micro Kit (Qiagen). RNA was reverse transcribed and amplified into cDNA using the Takara SmartSeq kit at the University of California (UC), Berkeley, QB3 Genomics Center, where library construction and sequencing were performed. See supplemental information for details.

### Principal-component analysis and clustering analysis

PCA and gene hierarchical clustering analysis were performed using R version 3.5.0, and described in detail in supplemental information.

### CUT&RUN

Organoids cultured under R and RD-7 conditions were harvested 5 days after initial plating. CUT&RUN was performed on the basis of the published protocol (Skene et al., 2018) with modifications. See supplemental information for details of procedures and library preparation. Samples were sequenced on the NextSeq345 system at the UC Davis Genomics Center.

### CUT&RUN analysis

Raw CUT&RUN reads were checked by FastQC version 0.11.8 for quality control to ensure the high-quality of data. Fastq files of the three biological replicates for each treatment condition and antibody pair were merged for downstream analyses. Peak calling, motif analysis, and visualization were performed as described in supplemental information.

### Functional enrichment analyses

Enriched biological themes from RNA-seq and CUT&RUN data were identified using the DAVID website (https://david.ncifcrf.gov). Gene set enrichment analysis was performed using GSEA software version 4.0.3. See supplemental information for details.

## SUPPLEMENTAL INFORMATION

Supplemental information can be found online at https://doi.org/10.1016/j.stemcr.2023.04.003.

## AUTHOR CONTRIBUTIONS

C.H., Y.L., and Z.A.W. designed the study. C.H. performed mouse experiments. C.H. and J.T. performed CUT&RUN experiments. Y.L. performed organoid experiments and RNA-seq. J.W. performed all bioinformatic analyses. J.G. helped with IF staining and lineage analysis. All authors discussed data. Z.A.W., C.H., Y.L., and J.W. prepared figures and wrote the manuscript.

## ACKNOWLEDGMENTS

We thank Lindsay Hinck for discussion of the study and the microscopy and fluorescence-activated cell sorting (FACS) shared facilities at UCSC and the genomics facilities at UC Davis and Berkeley for technical support. This work was supported by a post-doctoral fellowship from the TRDRP of California to Y.L. and NIH grants R01GM116872 and R01CA271452 to Z.A.W.

## CONFLICT OF INTERESTS

The authors declare no competing interests.

Received: December 13, 2022
Revised: April 6, 2023
Accepted: April 11, 2023
Published: May 11, 2023

## REFERENCES

Amir, A.L., Barua, M., McKnight, N.C., Cheng, S., Yuan, X., and Balk, S.P. (2003). A direct beta-catenin-independent interaction between androgen receptor and T cell factor 4. J. Biol. Chem. *278*, 30828–30834.

Bailey, T.L., Boden, M., Buske, F.A., Frith, M., Grant, C.E., Clementi, L., Ren, J., Li, W.W., and Noble, W.S. (2009). Meme SUITE: tools for motif discovery and searching. Nucleic acids research *37*, W202–W208.

Binnerts, M.E., Kim, K.A., Bright, J.M., Patel, S.M., Tran, K., Zhou, M., Leung, J.M., Liu, Y., Lomas, W.E., 3rd, Dixon, M., et al. (2007). R-Spondin1 regulates Wnt signaling by inhibiting internalization of LRP6. Proc. Natl. Acad. Sci. USA *104*, 14700–14705.

Brault, V., Moore, R., Kutsch, S., Ishibashi, M., Rowitch, D.H., McMahon, A.P., Sommer, L., Boussadia, O., and Kemler, R. (2001). Inactivation of the beta-catenin gene by Wnt1-Cre-mediated deletion results in dramatic brain malformation and failure of craniofacial development. Development *128*, 1253–1264.

Bruxvoort, K.J., Charbonneau, H.M., Giambernardi, T.A., Goolsby, J.C., Qian, C.N., Zylstra, C.R., Robinson, D.R., Roy-Burman, P., Shaw, A.K., Buckner-Berghuis, B.D., et al. (2007). Inactivation of Apc in the mouse prostate causes prostate carcinoma. Cancer Res. *67*, 2490–2496.

Chesire, D.R., Ewing, C.M., Gage, W.R., and Isaacs, W.B. (2002). In vitro evidence for complex modes of nuclear beta-catenin signaling during prostate growth and tumorigenesis. Oncogene *21*, 2679–2694.

Cheung, A.F., Carter, A.M., Kostova, K.K., Woodruff, J.F., Crowley, D., Bronson, R.T., Haigis, K.M., and Jacks, T. (2010). Complete deletion of Apc results in severe polyposis in mice. Oncogene *29*, 1857–1864.

Choi, N., Zhang, B., Zhang, L., Ittmann, M., and Xin, L. (2012). Adult murine prostate basal and luminal cells are self-sustained lineages that can both serve as targets for prostate cancer initiation. Cancer Cell *21*, 253–265.

Choi, Y.S., Zhang, Y., Xu, M., Yang, Y., Ito, M., Peng, T., Cui, Z., Nagy, A., Hadjantonakis, A.K., Lang, R.A., et al. (2013). Distinct functions for Wnt/β-catenin in hair follicle stem cell proliferation and survival and interfollicular epidermal homeostasis. Cell Stem Cell *13*, 720–733.

Clevers, H., Loh, K.M., and Nusse, R. (2014). Stem cell signaling. An integral program for tissue renewal and regeneration: Wnt signaling and stem cell control. Science *346*, 1248012.

Cunha, G.R., Alarid, E.T., Turner, T., Donjacour, A.A., Boutin, E.L., and Foster, B.A. (1992). Normal and abnormal development of the male urogenital tract. Role of androgens, mesenchymal-epithelial interactions, and growth factors. J. Androl. *13*, 465–475.

De Marzo, A.M., Platz, E.A., Sutcliffe, S., Xu, J., Grönberg, H., Drake, C.G., Nakai, Y., Isaacs, W.B., and Nelson, W.G. (2007). Inflammation in prostate carcinogenesis. Nat. Rev. Cancer *7*, 256–269.

Drost, J., Karthaus, W.R., Gao, D., Driehuis, E., Sawyers, C.L., Chen, Y., and Clevers, H. (2016). Organoid culture systems for prostate epithelial and cancer tissue. Nat. Protoc. *11*, 347–358.

English, H.F., Santen, R.J., and Isaacs, J.T. (1987). Response of glandular versus basal rat ventral prostatic epithelial cells to androgen withdrawal and replacement. Prostate *11*, 229–242.

Evans, G.S., and Chandler, J.A. (1987). Cell proliferation studies in the rat prostate: II. The effects of castration and androgen-induced regeneration upon basal and secretory cell proliferation. Prostate *11*, 339–351.

Farin, H.F., Jordens, I., Mosa, M.H., Basak, O., Korving, J., Tauriello, D.V.F., de Punder, K., Angers, S., Peters, P.J., Maurice, M.M., and Clevers, H. (2016). Visualization of a short-range Wnt gradient in the intestinal stem-cell niche. Nature *530*, 340–343.

Ferrer-Vaquer, A., Piliszek, A., Tian, G., Aho, R.J., Dufort, D., and Hadjantonakis, A.K. (2010). A sensitive and bright single-cell resolution live imaging reporter of Wnt/ss-catenin signaling in the mouse. BMC Dev. Biol. *10*, 121.

Francis, J.C., Thomsen, M.K., Taketo, M.M., and Swain, A. (2013). beta-catenin is required for prostate development and cooperates with Pten loss to drive invasive carcinoma. PLoS Genet. *9*, e1003180.

Fredriksson, S., Gullberg, M., Jarvius, J., Olsson, C., Pietras, K., Gústafsdóttir, S.M., Ostman, A., and Landegren, U. (2002). Protein detection using proximity-dependent DNA ligation assays. Nat. Biotechnol. *20*, 473–477.

Guerrero, J., Alfaro, I.E., Gómez, F., Protter, A.A., and Bernales, S. (2013). Enzalutamide, an androgen receptor signaling inhibitor, induces tumor regression in a mouse model of castration-resistant prostate cancer. Prostate *73*, 1291–1305.

Holland, J.D., Klaus, A., Garratt, A.N., and Birchmeier, W. (2013). Wnt signaling in stem and cancer stem cells. Curr. Opin. Cell Biol. *25*, 254–264.

Horton, C., Liu, Y., Yu, C., Xie, Q., and Wang, Z.A. (2019). Luminal-contact-inhibition of epithelial basal stem cell multipotency in prostate organogenesis and homeostasis. Biol. Open *8*, bio045724.

Huang, D.W., Sherman, B.T., and Lempicki, R.A. (2009). Bioinformatics enrichment tools: paths toward the comprehensive functional analysis of large gene lists. Nucleic Acids Res. *37*, 1–13.

Jean-Faucher, C., Berger, M., de Turckheim, M., Veyssiere, G., and Jean, C. (1978). Developmental patterns of plasma and testicular testosterone in mice from birth to adulthood. Acta Endocrinol. *89*, 780–788.

Julio, M.K., Shibata, M., Desai, N., Reynon, M., Halili, M.V., Hu, Y.P., Price, S.M., Abate-Shen, C., and Shen, M.M. (2013). Canonical Wnt signaling regulates Nkx3.1 expression and luminal epithelial differentiation during prostate organogenesis. Dev. Dyn. *242*, 1160–1171.

Karthaus, W.R., Iaquinta, P.J., Drost, J., Gracanin, A., van Boxtel, R., Wongvipat, J., Dowling, C.M., Gao, D., Begthel, H., Sachs, N., et al. (2014). Identification of multipotent luminal progenitor cells in human prostate organoid cultures. Cell *159*, 163–175.

Kishimoto, J., Burgeson, R.E., and Morgan, B.A. (2000). Wnt signaling maintains the hair-inducing activity of the dermal papilla. Genes Dev. *14*, 1181–1185.

Kwon, O.J., Zhang, B., Zhang, L., and Xin, L. (2016). High fat diet promotes prostatic basal-to-luminal differentiation and accelerates initiation of prostate epithelial hyperplasia originated from basal cells. Stem Cell Res. *16*, 682–691.

Kwon, O.J., Zhang, L., Ittmann, M.M., and Xin, L. (2013). Prostatic inflammation enhances basal-to-luminal differentiation and accelerates initiation of prostate cancer with a basal cell origin. Proc. Natl. Acad. Sci. USA *111*, E592–E600.

Lai, K.P., Yamashita, S., Vitkus, S., Shyr, C.R., Yeh, S., and Chang, C. (2012). Suppressed prostate epithelial development with impaired branching morphogenesis in mice lacking stromal fibromuscular androgen receptor. Mol. Endocrinol. *26*, 52–66.

Lee, E., Ha, S., and Logan, S.K. (2015). Divergent androgen receptor and beta-catenin signaling in prostate cancer cells. PLoS One *10*, e0141589.

Lu, T.L., and Chen, C.M. (2015). Differential requirements for beta-catenin in murine prostate cancer originating from basal versus luminal cells. J. Pathol. *236*, 290–301.

Machanick, P., and Bailey, T.L. (2011). MEME-ChIP: motif analysis of large DNA datasets. Bioinformatics *27*, 1696–1697.

Masiello, D., Chen, S.Y., Xu, Y., Verhoeven, M.C., Choi, E., Hollenberg, A.N., and Balk, S.P. (2004). Recruitment of beta-catenin by wild-type or mutant androgen receptors correlates with ligand-stimulated growth of prostate cancer cells. Mol. Endocrinol. *18*, 2388–2401.

Mulholland, D.J., Cheng, H., Reid, K., Rennie, P.S., and Nelson, C.C. (2002). The androgen receptor can promote beta-catenin nuclear translocation independently of adenomatous polyposis coli. J. Biol. Chem. *277*, 17933–17943.

Mulholland, D.J., Read, J.T., Rennie, P.S., Cox, M.E., and Nelson, C.C. (2003). Functional localization and competition between the androgen receptor and T-cell factor for nuclear beta-catenin: a means for inhibition of the Tcf signaling axis. Oncogene *22*, 5602–5613.

Mulholland, D.J., Tran, L.M., Li, Y., Cai, H., Morim, A., Wang, S., Plaisier, S., Garraway, I.P., Huang, J., Graeber, T.G., and Wu, H. (2011). Cell autonomous role of PTEN in regulating castration-resistant prostate cancer growth. Cancer Cell *19*, 792–804.

Ousset, M., Van Keymeulen, A., Bouvencourt, G., Sharma, N., Achouri, Y., Simons, B.D., and Blanpain, C. (2012). Multipotent and unipotent progenitors contribute to prostate postnatal development. Nat. Cell Biol. *14*, 1131–1138.

Pawlowski, J.E., Ertel, J.R., Allen, M.P., Xu, M., Butler, C., Wilson, E.M., and Wierman, M.E. (2002). Liganded androgen receptor interaction with beta-catenin: nuclear co-localization and modulation of transcriptional activity in neuronal cells. J. Biol. Chem. *277*, 20702–20710.

Poling, M.C., and Kauffman, A.S. (2012). Sexually dimorphic testosterone secretion in prenatal and neonatal mice is independent of kisspeptin-Kiss1r and GnRH signaling. Endocrinology *153*, 782–793.

Robinson, D., Van Allen, E.M., Wu, Y.M., Schultz, N., Lonigro, R.J., Mosquera, J.M., Montgomery, B., Taplin, M.E., Pritchard, C.C., Attard, G., et al. (2015). Integrative clinical genomics of advanced prostate cancer. Cell *161*, 1215–1228.

Schaeffer, E.M., Marchionni, L., Huang, Z., Simons, B., Blackman, A., Yu, W., Parmigiani, G., and Berman, D.M. (2008). Androgen-induced programs for prostate epithelial growth and invasion arise in embryogenesis and are reactivated in cancer. Oncogene *27*, 7180–7191.

Sfanos, K.S., Yegnasubramanian, S., Nelson, W.G., and De Marzo, A.M. (2018). The inflammatory microenvironment and microbiome in prostate cancer development. Nat. Rev. Urol. *15*, 11–24.

Simons, B.W., Hurley, P.J., Huang, Z., Ross, A.E., Miller, R., Marchionni, L., Berman, D.M., and Schaeffer, E.M. (2012). Wnt signaling though beta-catenin is required for prostate lineage specification. Dev. Biol. *371*, 246–255.

Skene, P.J., Henikoff, J.G., and Henikoff, S. (2018). Targeted in situ genome-wide profiling with high efficiency for low cell numbers. Nat. Protoc. *13*, 1006–1019.

Skene, P.J., and Henikoff, S. (2017). An efficient targeted nuclease strategy for high-resolution mapping of DNA binding sites. Elife *6*, e21856.

Söderberg, O., Leuchowius, K.J., Gullberg, M., Jarvius, M., Weibrecht, I., Larsson, L.G., and Landegren, U. (2008). Characterizing proteins and their interactions in cells and tissues using the in situ proximity ligation assay. Methods *45*, 227–232.

Song, L.N., Herrell, R., Byers, S., Shah, S., Wilson, E.M., and Gelmann, E.P. (2003). Beta-catenin binds to the activation function 2 region of the androgen receptor and modulates the effects of the N-terminal domain and TIF2 on ligand-dependent transcription. Mol. Cell Biol. *23*, 1674–1687.

Subramanian, A., Tamayo, P., Mootha, V.K., Mukherjee, S., Ebert, B.L., Gillette, M.A., Paulovich, A., Pomeroy, S.L., Golub, T.R., Lander, E.S., and Mesirov, J.P. (2005). Gene set enrichment analysis: a knowledge-based approach for interpreting genome-wide expression profiles. Proc. Natl. Acad. Sci. USA *102*, 15545–15550.

Terry, S., Yang, X., Chen, M.W., Vacherot, F., and Buttyan, R. (2006). Multifaceted interaction between the androgen and Wnt signaling pathways and the implication for prostate cancer. J. Cell. Biochem. *99*, 402–410.

Toivanen, R., Mohan, A., and Shen, M.M. (2016). Basal progenitors contribute to repair of the prostate epithelium following induced luminal anoikis. Stem Cell Rep. *6*, 660–667.

Toivanen, R., and Shen, M.M. (2017). Prostate organogenesis: tissue induction, hormonal regulation and cell type specification. Development *144*, 1382–1398.

Truica, C.I., Byers, S., and Gelmann, E.P. (2000). Beta-catenin affects androgen receptor transcriptional activity and ligand specificity. Cancer Res. *60*, 4709–4713.

van Amerongen, R., Bowman, A.N., and Nusse, R. (2012). Developmental stage and time dictate the fate of Wnt/β-catenin-responsive stem cells in the mammary gland. Cell Stem Cell *11*, 387–400.

Wang, Z.A., Mitrofanova, A., Bergren, S.K., Abate-Shen, C., Cardiff, R.D., Califano, A., and Shen, M.M. (2013). Lineage analysis of basal epithelial cells reveals their unexpected plasticity and supports a cell-of-origin model for prostate cancer heterogeneity. Nat. Cell Biol. *15*, 274–283.

Wei, X., Roudier, M.P., Kwon, O.J., Lee, J.D., Kong, K., Dumpit, R., True, L., Morrissey, C., Lin, D.W., Nelson, P.S., and Xin, L. (2022). Paracrine Wnt signaling is necessary for prostate epithelial proliferation. Prostate *82*, 517–530.

Wu, X., Daniels, G., Shapiro, E., Xu, K., Huang, H., Li, Y., Logan, S., Greco, M.A., Peng, Y., Monaco, M.E., et al. (2011). LEF1 identifies androgen-independent epithelium in the developing prostate. Mol. Endocrinol. *25*, 1018–1026.

Xie, Q., Liu, Y., Cai, T., Horton, C., Stefanson, J., and Wang, Z.A. (2017). Dissecting cell-type-specific roles of androgen receptor in prostate homeostasis and regeneration through lineage tracing. Nat. Commun. *8*, 14284.

Yang, F., Li, X., Sharma, M., Sasaki, C.Y., Longo, D.L., Lim, B., and Sun, Z. (2002). Linking beta-catenin to androgen-signaling pathway. J. Biol. Chem. *277*, 11336–11344.

Yokoyama, N.N., Shao, S., Hoang, B.H., Mercola, D., and Zi, X. (2014). Wnt signaling in castration-resistant prostate cancer: implications for therapy. Am. J. Clin. Exp. Urol. *2*, 27–44.

Yu, X., Wang, Y., Jiang, M., Bierie, B., Roy-Burman, P., Shen, M.M., Taketo, M.M., Wills, M., and Matusik, R.J. (2009). Activation of beta-Catenin in mouse prostate causes HGPIN and continuous prostate growth after castration. Prostate *69*, 249–262.

**Stem Cell Reports, Volume *18***

## Supplemental Information

# Modulation of the canonical Wnt activity by androgen signaling in prostate epithelial basal stem cells

**Corrigan Horton, Yueli Liu, Jiawen Wang, Jonathan Green, Jeremiah Tsyporin, Bin Chen, and Zhu A. Wang**

## Supplemental Figures and Legends

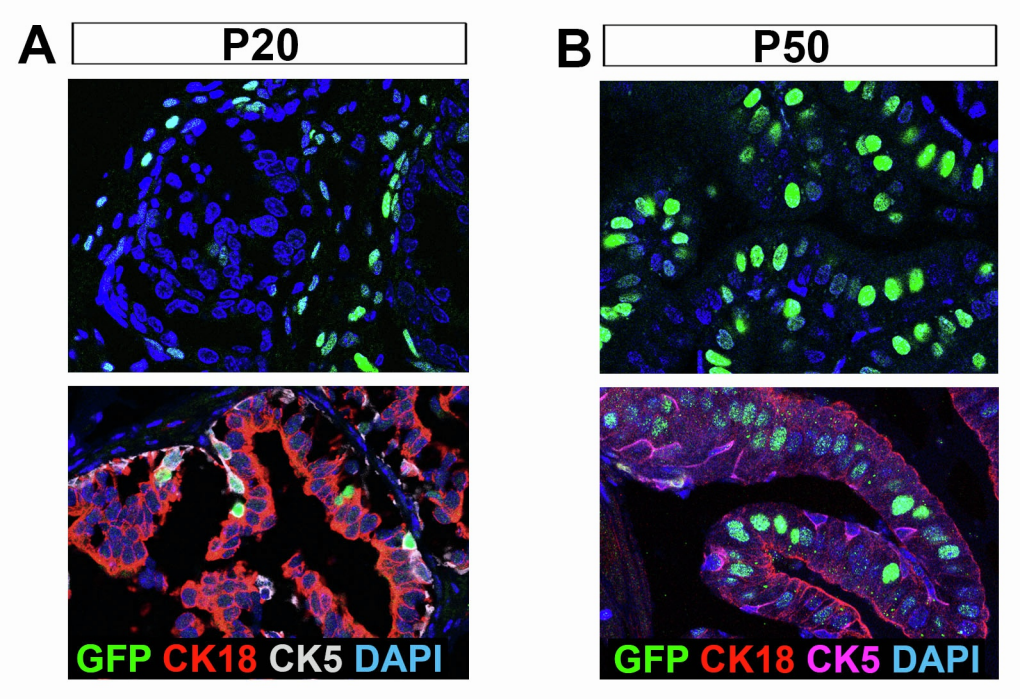


**Figure S1. Analysis of *TCF/Lef-H2B.GFP* expression pattern in prostate of different stages.**

(A) Representative direct visualization (upper panel) and IF staining (lower panel) images showing GFP signals in the stromal and basal cells of prostate ductal tips at P20. (B) Representative direct visualization (upper panel) and IF staining (lower panel) images showing GFP signals mostly present in the luminal cells at P50.

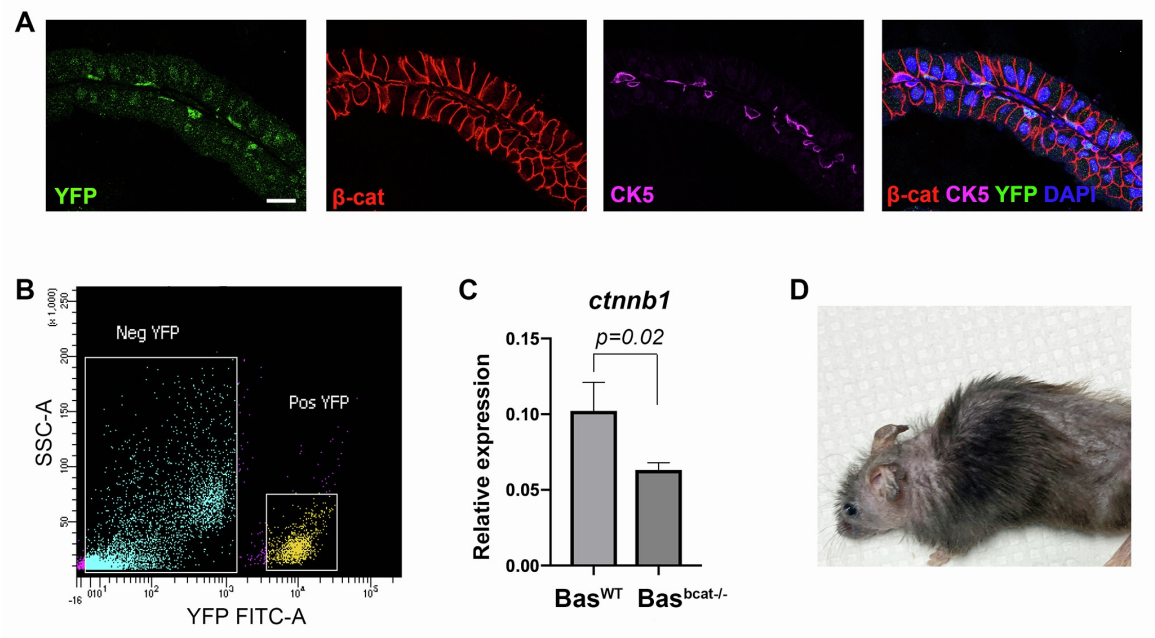


**Figure S2. Analysis of *Bas*$^{bcat-/-}$ basal cells.**

(**A**) IF images showing β-catenin expression pattern in *Bas*$^{bcat-/-}$ mice. Scale bar, 20 μm. (**B**) Representative FACS plot of sorting YFP+ *Bas*$^{bcat-/-}$ basal cells. (**C**) qRT-PCR showing significantly reduced β-catenin expression in *Bas*$^{bcat-/-}$ basal cells compared to wildtype basal cells by student's t-test. N=4 sorted cell samples each from an individual mouse per group. Gene expression levels were normalized to β-actin expression. Error bars correspond to one s.d. (**D**) A mouse losing hair due to β-catenin deletion by the *CK5-CreER*$^{T2}$ driver expression in skin basal cells.

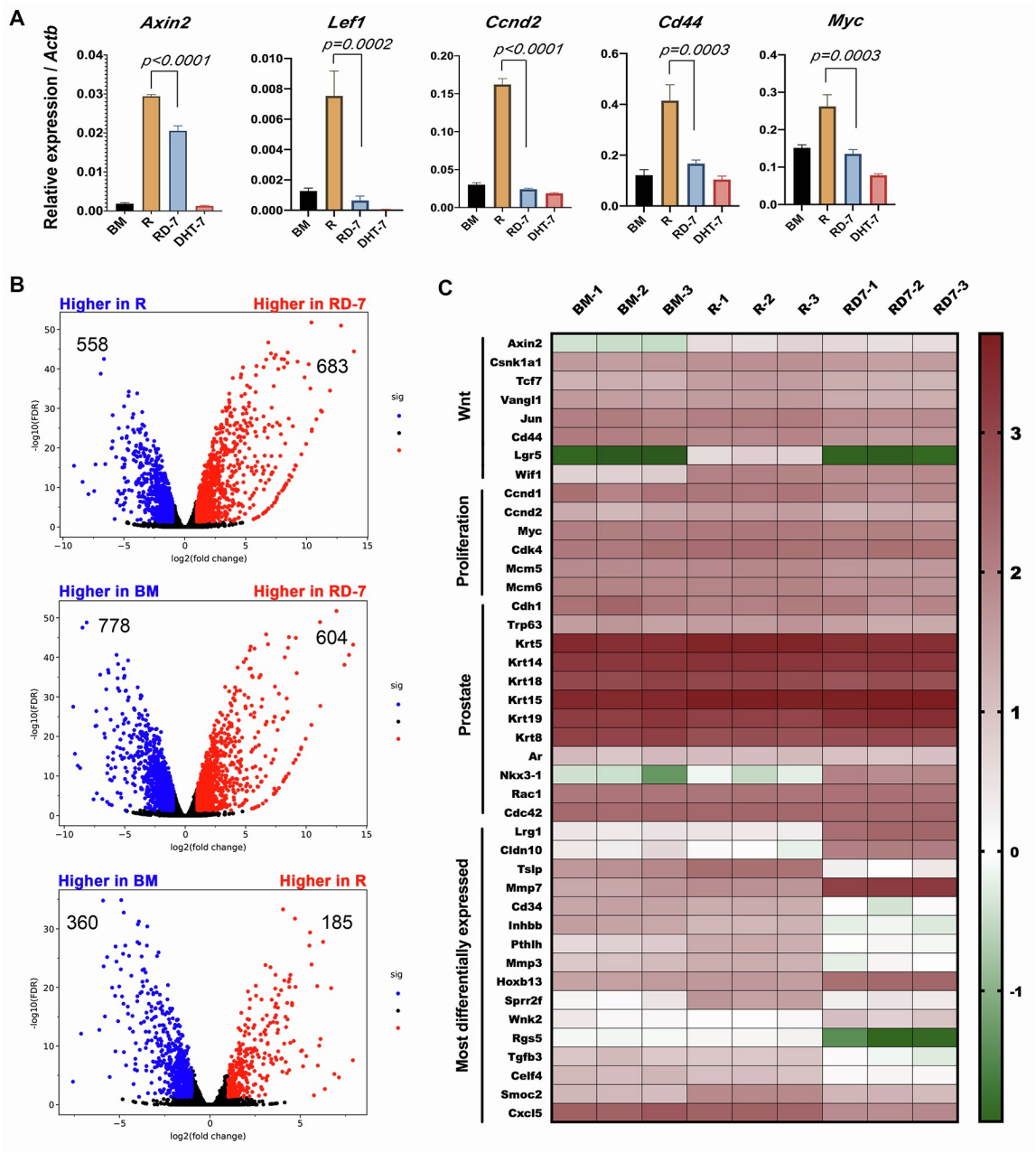


**Figure S3. Comparison of organoid RNA-seq data of different treatments.**

(**A**) qRT-PCR analysis of Wnt target genes under different treatments. Gene expression levels were normalized to β-actin expression. N=4 organoid samples cultured in separate batches for each group. *P* values calculated by student's *t*-test. Error bars correspond to one s.d. (**B**) Volcano plots showing the numbers of upregulated and downregulated genes between R vs. BM, RD-7 vs. R, and BM vs. RD-7 (FDR<0.05 and fold change >2 or <-2). (**C**) Heatmap showing expression levels of selected genes in different samples.

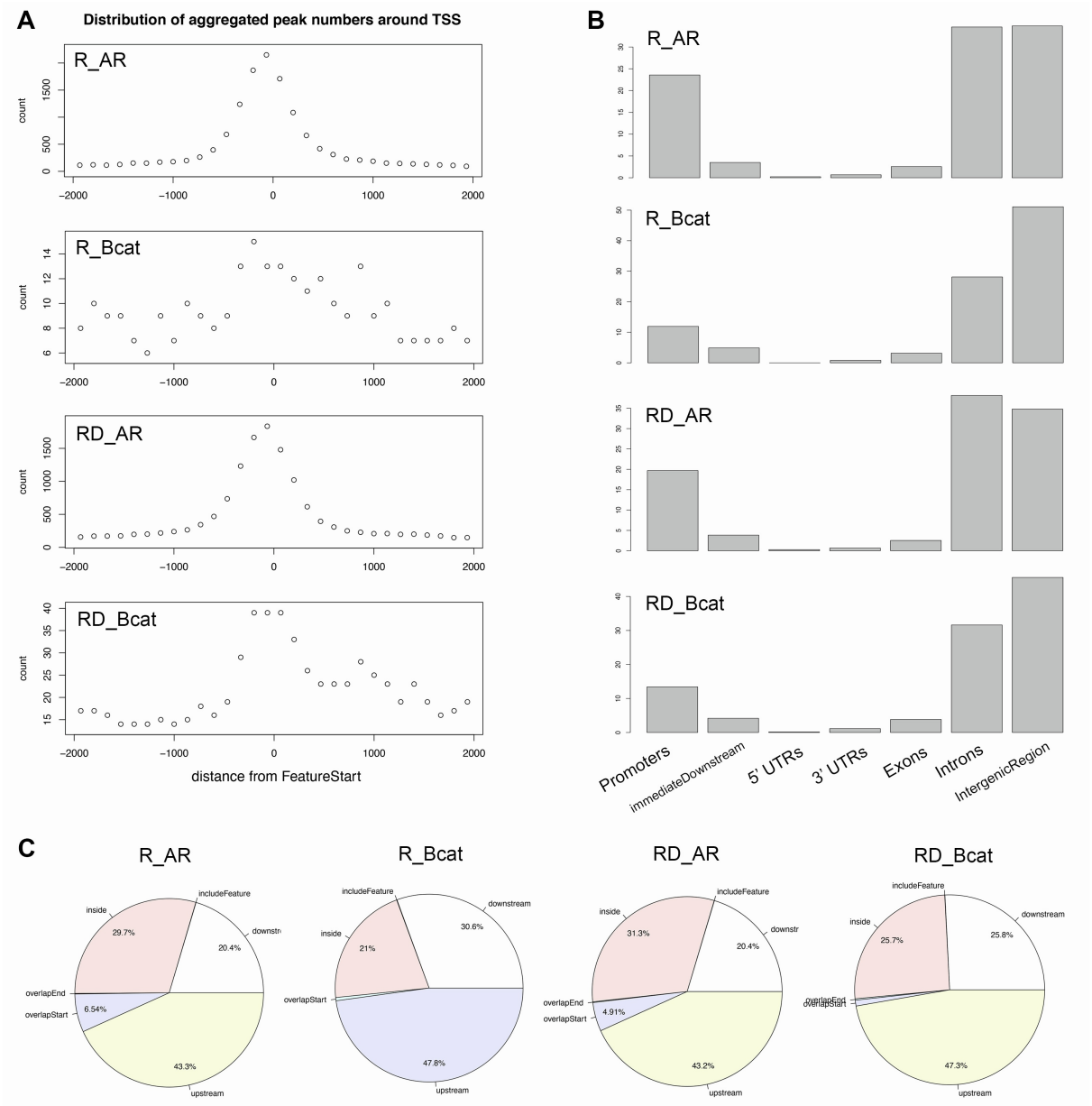


**Figure S4. Summary of annotation of called peaks for the CUT&RUN samples.**

(**A**) Plot showing the number of peak distributions of the distances to the transcription start sites (TSS) for each sample. (**B**) Bar graph showing the percentages of the peaks over promoters, 5' UTR, exons, introns, 3' UTRs, immediate downstream, and intergenic region for each sample. (**C**) Pie chart showing the distributions of peak position relative to the features of the nearest gene for each sample.

## Supplemental Tables

### Table S2. Primers used in this study

Primers for mouse genotyping

| Alleles | Primer Sequences | |
|---|---|---|
| *CreER$^{T2}$* | Forward | 5'-CAGATGGCGCGGCAACACC-3' |
| | Reverse | 5'-GCGCGGTCTGGCAGTAAAAAC-3' |
| *R26R-CAG-YFP* | Wild-type Forward | 5'-AAAGTCGCTCTGAGTTGTTAT-3' |
| | Wild-type Reverse | 5'-CCGAAAATCTGTGGGAAGTC-3' |
| | Mutant Forward | 5'-ACATGGTCCTGCTGGAGTTC-3' |
| | Mutant Reverse | 5'-GGCATTAAGCAGCGTATCC-3' |
| *ctnnb1$^{fl/fl}$* | Forward | 5'-ACTGCCTTTGTTCTCTTCCCTTCTG-3' |
| | Reverse | 5'-CAGCCAAGGAGAGCAGGTGAGG-3' |
| *Pten$^{fl/fl}$* | Forward | 5'-ACTCAAGGCAGGGATGAGC-3' |
| | Reverse | 5'-GTCATCTTCACTTAGCCATTGG-3' |
| *APC$^{fl/fl}$* | Forward | 5'-GAGAAACCCTGTCTCGAAAAAA-3' |
| | Reverse | 5'-AGTGCTGTTTCTATGAGTCAA-3' |
| *TCF-H2B.GFP* | Forward | 5'-ACAACAAGCGCTCGACCATCAC-3' |
| | Reverse | 5'-AGTCGATGCCCTTGAGCTCGAT-3' |

Primers for qPT-PCR

| Genes | Primer sequence | |
|---|---|---|
| *Axin2* | forward | 5’-CAGAGGGACAGGAACCACTC-3’ |
| | reverse | 5’-TGGACACTTGCCAGTTTCTT-3’ |
| *Lef1* | forward | 5’-ACGACAAGGCCAGAGAACA-3’ |
| | reverse | 5’-GTCGCTGTTCATATTGGGCA-3’ |
| *Ccnd2* | forward | 5’-AAGGACCGGTGCGAGTCA-3’ |
| | reverse | 5’-GGGAGTGCTTCCCTTACCTC-3’ |
| *Cd44* | forward | 5’-TCGATTTGAATGTAACCTGCCG-3’ |
| | reverse | 5’-CAGTCCGGGAGATACTGTAGC-3’ |
| *Myc* | forward | 5’-CCCTAGTGCTGCATGAGGA-3’ |
| | reverse | 5’-TGCCTCTTCTCCACAGACAC-3’ |
| *Ctnnb1* | forward | 5’-CATCCCACTGGCCTCTGATA-3’ |
| | reverse | 5’-TCGTGGAATAGCACCCTGTT-3’ |
| *Actb* | forward | 5’-CGCCACCAGTTCGCCATGGA-3’ |
| | reverse | 5’-TACAGCCCGGGGAGCATCGT-3’ |

**Table S3. Antibodies used in this study**

Antibodies for flow cytometry

| Antibody | Supplier | Dilution |
|---|---|---|
| Sca-1-PE-Cy7 | Biolegend clone E13-161.7 #122513 | 1:500 |
| CD49f-PE | eBiosciences clone eBioGoH3 #12-0495 | 1:300 |
| Ter119-eFluor450 | eBiosciences clone Ter119 #48-5921 | 1:250 |
| CD31-eFluor450 | eBiosciences clone 390 #48-0311 | 1:250 |
| CD45-eFluor450 | CD45-eFluor450eBiosciences clone 30-F11 #48-0451 | 1:250 |

Primary antibodies used for immunofluorescence staining and Duolink PLA

| Antigen | Supplier | Ig type | Dilution |
|---|---|---|---|
| BrdU | Serotec #MCA2060 | Rat IgG2a | 1:500 |
| Ki67 | DakoCytomation #M7249 | Rat IgG2a | 1:600 |
| YFP | Abcam #13970 | Chick IgY | 1:2000 |
| CK5 | Covance #PRB-160P | Rabbit IgG | 1:1000 |
| CK18 | Abcam #ab668 | Mouse IgG1 | 1:200 |
| p63 | GeneTex #GTX102425 | Rabbit IgG | 1:1000 |
| AR | Sigma #A9853 | Rabbit IgG | 1:500 |
| β-catenin | BD Biosciences #610153 | Mouse IgG1 | 1:500 for Duolink 1:1000 for IF |

Antibodies used for CUT&RUN

| Antigen | Supplier | Ig type | Dilution |
|---|---|---|---|
| AR | Abcam #ab108341 | Rabbit IgG | 1:100 |
| Active β-catenin | Cell Signaling #8814 (D13A1) | Rabbit IgG | 1:100 |

## Experimental Procedures

### Mouse procedures

For tamoxifen induction, mice were administered 9 mg per 40 g body weight tamoxifen (Sigma) suspended in corn oil by oral gavage once daily for 4 consecutive days. For BrdU incorporation assay, BrdU (Sigma) was dissolved in PBS (10 mg/ml) and administered by intraperitoneal injection twice daily (0.1 ml per dose) for 11 consecutive days during homeostasis to label proliferating cells. For androgen pump implantation, a mini-osmotic pump (Alzet) filled with testosterone (25 mg/ml in 100% ethanol and diluted in PEG-400 to a final concentration of 7.5 mg/ml) was subcutaneously implanted.

### Tissue collection and flow cytometry

Mouse prostate tissues were dissected and fixed in 4% paraformaldehyde for subsequent cryo-embedding in OCT compound (Sakura), or fixed in 10% formalin followed by paraffin embedding. For flow cytometry, prostate tissues were dissected and minced to small clumps, followed by enzymatic dissociation with 0.2% Collagenase/Hyaluronidase (StemCell Technologies) in DMEM/F12 media with 5% FBS for 3 h at 37°C. Tissues were digested with 0.25% Trypsin-EDTA (StemCell Technologies) for 1 h at 4°C, passed through 21- to 26-gauge syringes and filtered through a 40-mm cell strainer to obtain single-cell suspensions. Dissociated prostate cells were suspended in Hanks' Balanced Salt Solution Modified/2% FBS. Dead cells were excluded by propidium iodide staining.

### Renal grafting assay

Flow-sorted $APC^{fl/fl}$ $YFP^{+}$ basal cells were mixed with $2.5 \times 10^5$ dissociated urogenital sinus mesenchyme (UGM) cells from embryonic day 18.0 rat embryos. UGM cells were obtained from dissected urogenital sinus treated for 30 min in 1%

trypsin, followed by mechanical dissociation and treatment with 0.1% collagenase B (Roche) for 30 min at 37°C, and washing in PBS. Pelleted cell mixtures were resuspended in 10 µl of 1:9 collagen/setting buffer (10× Earle's Balanced Salt Solution (Life Technologies), 0.2 M $NaHCO_3$ and 50 mM NaOH), and gelatinized at 37°C for 20 min. Tissue recombinants were cultured in DMEM/10% FBS supplemented with $10^{-7}$ M DHT overnight, followed by transplantation under the kidney capsules of immunodeficient NCRNU-M sp/sp nude mice (Taconic Biosciences).

**Prostate organoids culture**

For mouse prostate organoid formation, flow-sorted basal cells were washed with advanced DMEM/F12 (Life Technologies), and resuspended in 10 µl advanced DMEM/F12 and 30 µl Matrigel per well in the Nunc Lab-Tek II CC2 Chamber Slide System (Thermo Fisher Scientific). Chamber slide was put upside down in the 37°C cell culture incubator for 15 min to let the matrigel solidify. For organoid culture, the following components were added to advanced DMEM/F12 medium: B27 (50× diluted), HEPES 1 M (100× diluted), GlutaMAX (100× diluted), Penicillin-streptomycin (100× diluted), N-acetylcysteine (1.25 mM), EGF (50 ng/ml), A83-01 (200 nM), Noggin (100 ng/ml), Y-27632 dihydrochloride (10 µM) as basement medium (BM). R-spondin1 (500 ng/ml) and different concentrations of DHT ($10^{-7}$M, $10^{-9}$M) were added alone or in combinations to BM as different treatments. Organoid culture medium was pre-warmed before adding to the wells. The medium was changed every 3 days. Organoids were fixed in 4% PFA for 20 min at room temperature before IF staining.

**Immunofluorescence staining**

Immunofluorescence staining was performed using 6 μm cryosections or on organoids in situ. Samples were incubated with 10% normal goat serum (NGS) and primary antibodies diluted in 10% NGS overnight at 4°C. Samples were then incubated with secondary antibodies (diluted 1:500 in PBST) labeled with Alexa Fluor 488, 555, or 647 (Invitrogen/Molecular Probes). Slides were mounted with VectaShield mounting medium with DAPI (Vector Labs), and images were taken on a Leica TCS SP5 spectral confocal microscope in the UCSC Microscopy Shared Facility.

**Lineage Analysis**

For lineage-tracing analysis, cell numbers were counted manually using confocal 40x photomicrographs across tissue sections. Basal cells were determined based on positive CK5 staining and location at the basement membrane. Luminal cells were determined based on positive CK18 staining, the columnar shape, and location at the apical side of the epithelium.

**Organoid bulk RNA-seq and analysis**

The 2x150 bp paired-end sequencing was performed on the NovaSeq 6000 platform. Sequencing reads were mapped to mouse genome (mm10) using the STAR package. Mapped sequencing reads were assigned to genes using 'featurecounts' function of Rsubread package (version 1.30.7). Expression of genes was measured by calculating fragments per kilobase of exon model per million mapped reads (FPKM value) using edgeR package (version 3.24.1) with default settings. Differential expression was estimated using the empirical Bayes methods (edgeR v3.24.1 in R v3.5.0) to obtain false discovery rate (FDR) and fold change.

**Principal components analysis and clustering analysis**

Genes with extremely low or high expression (the mean FPKM in all samples < 0.3 or > 6000) were filtered out to decrease data noise and potential outliers. The log-transformation was performed on the data. PCA was then performed on the data with 'prcomp' function in R v3.5.0 with the parameter scale. = TRUE. The gene hierarchical clustering was done by using 'heatmap.2' function of gplots package (version 3.0.1 in R v3.5.0). Here, the Spearman correlation distance was calculated and the complete linkage clustering algorithm was chosen.

**CUT&RUN**

Organoids were enzymatically dissociated into single cells by incubation in pre-warmed TrypLE (Invitrogen) at 37°C for 20 min with disruption by pipetting every 7 min. Dissociated cells were spun down at 600g and resuspended in ice cold Wash Buffer (20mM HEPES pH 7.5, 150mM NaCl, 0.5mM Spermidine, 1X EDTA-free protease inhibitor, Roche, 04693159001). Three washes were completed. After counting, 500,000 cells isolated from 4 wells were used to bind to 10µL Concanavalin-A beads (Cell Signaling, 93569) in each tube. Three tubes (biological replicates) were performed for each treatment condition and antibody pair. Cells bound to beads were incubated with the appropriate antibody at a concentration of 1:100, in 150µL antibody buffer (Wash Buffer with 2mM EDTA, 0.03% Digitonin, MilliporeSigma, 300410) at 4°C overnight with shaking at 400rpm. Beads were then washed twice with DIG-Wash Buffer (Wash Buffer with 0.03% Digitonin), and incubated with protein A/G-MNase (EpiCypher, 15-1016) for 1 hour at 4°C. Beads were washed twice and then Protein A/G-MNase was activated by adding $Ca^{2+}$ to a final concentration of 1mM and incubating at 0°C for 1 hour in a heat block immersed in an ice water slurry. The reaction was stopped by adding 100µL 2X STOP Buffer (170mM NaCl, 20mM EGTA, 0.05%, 50µg/mL RNAse A, 20µg/mL Glycogen,

250pg *E. coli* Spike-in DNA, EpiCypher 18-1401). Samples were then incubated at 37°C for 30 min, and supernatant was transferred to fresh tubes. Phenol chloroform isoamyl alcohol extraction was performed to purify CUT&RUN DNA, which was resuspended in 30µL 1mM Tris-HCl pH 8.0, 0.1mM EDTA.

CUT&RUN library preparation was performed for each tube using the NEBNext Ultra II DNA Library Prep Kit with modifications to the protocol. For the adapter ligation step, the NEBNext Adaptor for Illumina was diluted 1:50, to 0.3µM. The adaptor ligated DNA was then cleaned up with 2.1X AMPure XP beads before proceeding. PCR was performed with NEBNext Multiplex Oligos for Illumina (E7600S) with the following thermocycler conditions: Initial denaturation 98°C, 30s, denaturation 98°C, 10s, annealing and extension 65°C, 12s, repeat denaturing and annealing and extension 14 times, final extension 65°C, 5 minutes. 0.5X AMPure beads were added to the reaction, mixed, incubated for 10 minutes, and samples were placed on a magnet stand. Supernatant was transferred to fresh tubes and then cleaned up with 2X AMPure beads. DNA concentrations were determined using Bioanalyzer High Sensitivity DNA kit (5067-4626). Samples were pooled such that equimolar amounts of each sample were present. Samples were sequenced on the NextSeq345 system at the UC Davis Genomics Center at a depth of ~30M reads per sample.

**Peak calling, motif analysis and visualization**

Fastq files of the three biological replicates for each treatment condition and antibody pair were merged for peak calling. Paired end reads were aligned with bowtie2 (v2.4.1) in very sensitive local mode (--very-sensitive-local --no-unal --no-mixed --no-discordant --phred33 –I 10 –X 700) using mm10 genome. Peak calling was performed using MACS2 (v2.2.7.1) with a threshold of $p<0.001$. The peaks signals were normalized as fragment pileup per million reads.

Overlapping peaks across different treatments were obtained using ChIPpeakAnno (v3.28.1) with default parameters (maximum gap of 1kb between the two peak lists). Peaks were then assigned to the nearest genes within 5 kb to the transcription start sites (TSS), which were generated from the TxDb.Mmusculus.UCSC.mm10.knownGene Annotation package. Binding patterns of raw signals of multiple CUT&RUN experiments were compared and visualized using function featureAlignedHeatmap and featureAlignedDistribution of ChIPpeakAnno. Peaks were sorted by fold change and the best 1000 peaks were retrieved. Deeptools (v2.30.0) was used for extracting DNA sequences of these peaks and MEME-ChIP was used for discovering de novo motifs.

**Functional enrichment analyses**

Over-representation analysis was performed using DAVID. The differentially expressed genes (FDR < 0.05, and fold change > 2 or <-2) were extracted and fed to the DAVID website (https://david.ncifcrf.gov/) to identify enriched biological themes, particularly GO terms. For CUT&RUN, gene lists of any interesting peak sets were used as input to the DAVID website.

Gene set enrichment analysis was performed using GSEA software v4.0.3. The significantly differentially expressed genes (FDR < 0.05) were ranked by their log-transformed fold change value. The pre-ranked gene list and MousePath_All_gmt-Format.gmt or MousePath_GO_gmt.gmt gene set (both were downloaded from http://ge-lab.org/gskb/) were used for running the tool “Run GSEA Preranked” with default parameters.